


Article

# Analysis of Garnet by Laser-Induced Breakdown Spectroscopy—Two Practical Applications

Peter A. Defnet<sup>1,2</sup>, Michael A. Wise<sup>3</sup>, Russell S. Harmon<sup>4,\*</sup> , Richard R. Hark<sup>2,5</sup>  and Keith Hilferding<sup>2</sup><sup>1</sup> Department of Chemistry, University of Washington, Seattle, WA 98195, USA; defnep@uw.edu<sup>2</sup> Department of Chemistry, Juniata College, Huntingdon, PA 16652, USA; richard.hark@yale.edu (R.R.H.); khilferding@gmail.com (K.H.)<sup>3</sup> Department of Mineral Sciences, National Museum of Natural History, Smithsonian Institution, Washington, DC 20560, USA; wisem@si.edu<sup>4</sup> Department of Marine, Earth and Atmospheric Sciences, North Carolina State University, Raleigh, NC 27695, USA<sup>5</sup> Institute for the Preservation of Cultural Heritage, Yale University, West Haven, CT 06516, USA

\* Correspondence: rsharmon@ncsu.edu; Tel.: +1-919-588-0613

**Abstract:** Laser-induced breakdown spectroscopy (LIBS) is a simple and straightforward technique of atomic emission spectroscopy that can provide multi-element detection and quantification in any material, in-situ and in real time because all elements emit in the 200–900 nm spectral range of the LIBS optical emission. This study evaluated two practical applications of LIBS—validation of labels assigned to garnets in museum collections and discrimination of LCT (lithium-cesium-tantalum) and NYF (niobium, yttrium and fluorine) pegmatites based on garnet geochemical fingerprinting, both of which could be implemented on site in a museum or field setting with a handheld LIBS analyzer. Major element compositions were determined using electron microprobe analysis for a suite of 208 garnets from 24 countries to determine garnet type. Both commercial laboratory and handheld analyzers were then used to acquire LIBS broadband spectra that were chemometrically processed by partial least squares discriminant analysis (PLSDA) and linear support vector machine classification (SVM). High attribution success rates (>98%) were obtained using PLSDA and SVM for the handheld data suggesting that LIBS could be used in a museum setting to assign garnet type quickly and accurately. LIBS also identifies changes in garnet composition associated with increasing mineral and chemical complexity of LCT and NYF pegmatites.

**Keywords:** garnet; laser-induced breakdown spectroscopy; LIBS; electron microprobe analysis; geochemical fingerprinting; chemometrics; PCA; PLSDA; SVM



**Citation:** Defnet, P.A.; Wise, M.A.; Harmon, R.S.; Hark, R.R.; Hilferding, K. Analysis of Garnet by Laser-Induced Breakdown Spectroscopy—Two Practical Applications. *Minerals* **2021**, *11*, 705. <https://doi.org/10.3390/min11070705>

Academic Editors: Daniel Sbarbaro, Eduardo Balladares and Jorge Yañez

Received: 2 June 2021

Accepted: 25 June 2021

Published: 29 June 2021

**Publisher's Note:** MDPI stays neutral with regard to jurisdictional claims in published maps and institutional affiliations.



**Copyright:** © 2021 by the authors. Licensee MDPI, Basel, Switzerland. This article is an open access article distributed under the terms and conditions of the Creative Commons Attribution (CC BY) license (<https://creativecommons.org/licenses/by/4.0/>).

## 1. Introduction

### 1.1. Laser-Induced Breakdown Spectroscopy (LIBS)

LIBS is a specific application of atomic emission spectroscopy that affords rapid, multi-element analysis of material in any physical state—gas, liquid, or solid [1]—and has particular attributes that make it a useful and highly versatile technique for the real-time, in-situ analysis of geological materials in both the laboratory and the field. LIBS instrumentation is both simple and robust and LIBS is simultaneously sensitive to all elements, the broadband spectrum measured from the plasma emission records the full chemical composition of a sample above each element's limit of detection, which is a unique geochemical fingerprint [2] of the material analyzed. Commercial LIBS technology has recently progressed from bespoke and commercial laboratory systems to handheld analyzers for field use. This new capability offers the possibility for using LIBS as a survey tool for distinguishing different geological materials through rapid compositional analysis outside the laboratory under ambient environmental conditions with little to no sample preparation.

Since its first application to geological materials in the early 1990s, LIBS has become an ever more popular tool for geochemical analysis across a broad spectrum of the geosciences. In LIBS, a high-intensity pulsed laser beam is focused onto the surface of a sample to create a high-temperature plasma as the consequence of the multi-stage breakdown process that occurs when laser energy couples to a material. Typically, a sub-milligram amount of the sample being analyzed is first ablated, vaporized, subsequently dissociated in the high-temperature plasma into a collection of free electrons plus weakly ionized molecular, atomic, and ionic species. Species recombination and de-excitation occurs as the plasma cools down, with light emitted at discrete wavelengths when energy is released as photons and electrons return to low-energy levels. Because many electron orbital transitions occur for most elements, a LIBS emission intensity spectrum consists of multiple peaks for the majority of elements and, for most geological materials, normally contains tens to hundreds of spectral lines. A broadband LIBS spectrum records the full elemental composition of a sample, since every element in the periodic table has one or more emission lines in the ultraviolet, visible, and near infrared spectral region between 200–900 nm. LIBS analysis has been used in four distinct ways: (i) as an elemental detector, (ii) for quantitative chemical analysis, (iii) for microscale elemental mapping, and (iv) qualitatively to rapidly distinguish between samples of similar character through chemometric analysis, e.g., via spectral matching against a pre-assembled library.

### 1.2. Garnet

Garnet is an important and widespread rock-forming mineral that occurs worldwide in four geological contexts: (i) as a primary component in the Earth's upper mantle and lower crust, (ii) as a common constituent in crustal metamorphic rocks, (iii) as an accessory mineral in sedimentary rocks and detrital sediments, and (iv) as a rare constituent in igneous rocks [3,4]. As the geologic setting typically determines the particular type of garnet(s) that form, compositional analysis has been widely used to determine the provenance of detrital garnet present in clastic sediments derived from the erosion of continental crust [5–8] and in the exploration for diamond-bearing kimberlites [9–12]. It also has potential in exploration for mineralized skarns [13–15]. Garnet has a host of industrial uses and is a common gem mineral. Therefore, garnet is frequently found in museum mineral collections.

## 2. Applications Investigated

This study evaluated two practical applications of the LIBS—the validation of labels assigned to garnets in museum collections and the discrimination of LCT and NYF granitic pegmatites based on garnet geochemical fingerprinting.

### 2.1. Specimen Labeling Issue in Museum Collections

Specimen labels in museum collections enable curators and researchers to quickly access vital information about particular objects of interest. For mineral collections, species names and the locality are the most important information that should be recorded on all specimen labels. This information allows scientists, curators and collectors to connect the specimen to its geological context and provenance and make inferences about the minerals' origins. Much of the scientific value of the specimen is lost if the species name and locality information is incorrect or absent. However, such information can frequently be lacking. For example, the National Mineral Collection at the Smithsonian Institution lists about 3500 specimens of natural garnet in its database, of which 111 are listed simply as garnet with no species designation. It is estimated that at least 90% of the nearly 3500 garnet specimens in the collection have never been chemically analyzed to verify their label description. We have also learned from the mineral collections manager of the Yale Peabody Museum of Natural History that half of museum's collection of >800 garnets have no compositional information, and the certainty of the labeled specimens is not known (S. Nicolescu, personal communication).

A variety of factors can lead to the mislabeling of mineral species names in museum collections including: (i) visual misidentification, (ii) reclassification and redefinition of species resulting in changes in nomenclature, (iii) qualitative or incomplete chemical analyses of the specimen, and (iv) unvalidated species identification acquired from sources outside of the museum and passed on to current museum collections by previous researchers, collectors, and mineral dealers. Using analytical techniques to correct misidentified or mislabeled mineral specimens helps to maintain the scientific integrity of the specimen and the collection as a whole. The first question examined in this study was: Can a handheld LIBS instrument be efficacious in the determination of garnet type for the validation or correction of museum specimen labels?

## 2.2. Pegmatite Discrimination

Granitic pegmatites are an important source of a broad suite of rare metallic elements essential to today's high-technology industries and also for certain bulk minerals [16,17]. Two geochemical families of mineralogically complex rare-element pegmatites having a granitic association are recognized—the Li–Cs–Ta (LCT) pegmatites and the Nb–Y–F (NYF) pegmatites. Quartz, potassium feldspar, and albite are the major constituents in both the LCT and NYF pegmatites, with muscovite, biotite, garnet, tourmaline, and apatite typically present as accessory phases.

Most LCT pegmatites occur worldwide in supracrustal rocks metamorphosed in the upper greenschist to lower amphibolite facies and are typically located in the vicinity of evolved, S-type peraluminous granites and leucogranites from which they are inferred to be derived by fractional crystallization [18]. Pegmatites of the LCT family are characterized by enrichment in Li, Rb, Cs, Be, Sn, Nb, Ta, B, P and F, but typically have low abundances of Ti, Zr, Y and the rare earth elements (REE). In chemically evolved LCT pegmatites, spodumene, petalite, and lepidolite are the major Li-bearing minerals. Beryl is the primary host mineral for Be, pollucite for Cs, the columbite group minerals for Nb and Ta, and cassiterite for Sn. LCT pegmatites are also a significant source of gem minerals and museum quality specimens of rare minerals. Exploration and assessment for LCT pegmatites are guided by a number of observations that include increasing contents of Li in white mica and increasing Mn in garnet. By contrast, NYF pegmatites typically have a subaluminous to metaluminous A-type granite association. These pegmatites generally contain chemically complex silicate and oxide minerals that are characteristically enriched in Sc, Ti, Y, Zr, Nb > Ta, REE, U, and Th, contain negligible P and B, and are impoverished in the alkali elements Li, Rb, and Cs [19]. The presence of F is documented by abundant fluorite or topaz.

## 3. Garnet

### 3.1. Garnet Mineralogy, Chemistry, and Classification

Garnet is a nesosilicate mineral constructed of isolated silicon tetrahedra ( $\text{SiO}_4$ ) connected by interstitial cations that has a generalized crystal chemical formula of  $X_3Y_2\text{Si}_3\text{O}_{12}$  [20], where X is a site of 8-fold coordination filled by solid solution of a divalent cation ( $\text{Fe}^{2+}$ ,  $\text{Ca}^{2+}$ ,  $\text{Mg}^{2+}$ ,  $\text{Mn}^{2+}$ ) and Y is a site of 6-fold coordination occupied by a trivalent cation ( $\text{Al}^{3+}$ ,  $\text{Fe}^{3+}$  or  $\text{Cr}^{3+}$ ). As recognized by Menzer [21], common natural occurrences of garnet are of six isostructural end-member types—almandine [ $\text{Fe}_3\text{Al}_2\text{Si}_3\text{O}_{12}$ ], pyrope [ $\text{Mg}_3\text{Al}_2\text{Si}_3\text{O}_{12}$ ], spessartine [ $\text{Mn}_3\text{Al}_2\text{Si}_3\text{O}_{12}$ ], andradite [ $\text{Ca}_3\text{Fe}_2\text{Si}_3\text{O}_{12}$ ], grossular [ $\text{Ca}_3\text{Al}_2\text{Si}_3\text{O}_{12}$ ], and uvarovite [ $\text{Ca}_3\text{Cr}_2\text{Si}_3\text{O}_{12}$ ]. Most natural garnets occur as multicomponent solid solutions involving X and Y site cations, although many additional end-member species and elemental substitutions exist in natural garnets such that the garnet supergroup comprise a total of 32 species [22]. The broad range of colors displayed by garnet, ranging across the spectrum from black, brown, red, pink, orange, yellow, and green is a consequence of transition element substitution in the X and Y structural sites [23].

### 3.2. Garnet Sample Suite

The suite of 208 garnets used for this study (Table A1, Appendix A) came from three sources: (i) 151 specimens from the collection of the Smithsonian's National Museum of Natural History (NMNH), (ii) 56 samples from the personal collection of one coauthor (RSH), and a single sample from the Weld pegmatite in Franklin County, Maine (USA) collected by another coauthor (MAW). These garnets originated from a wide range of igneous and metamorphic rock associations. Typically, different rock types contain garnet with distinctive chemical compositions.

Felsic igneous rocks that typically contain garnet include granitic pegmatites, rhyolites and syenites that all likely originated in the crust. Almandine and spessartine occur primarily in granitic pegmatite (e.g., Hawk Mine, NC, USA; Rutherford Mine, VA, USA; Little 3 Mine, Ramona, CA, USA; Golcando Mine, Minas Gerais State, Brazil) and rhyolite (e.g., Nathop, CO, USA; Topaz Mountain, UT, USA), whereas andradite is associated with syenite (e.g., Magnet Cove, AR, USA). Almandine, grossular, and spessartine are very common constituents of metamorphic rocks (e.g., Osgood Mountains, NV, USA; Sierra De Cruces, Coahuila, Mexico; Broken Hill, Australia; Ducktown Mine, TN, USA; Jeffrey Mine, QC, Canada). Garnetiferous kimberlite and chromitite are ultramafic igneous rocks probably generated in the upper mantle. Pyrope is the dominant garnet species from our kimberlite localities (e.g., Kimberly, South Africa; Garnet Ridge, AZ, USA), whereas uvarovite is generally associated with chromite pods (e.g., Saranovskii Mine, Russia).

Samples of garnet in medium- to high-grade metamorphic rocks, such as schist, gneiss and amphibolite, all have almandine compositions (e.g., Roxbury, CT, USA; Umba River Valley, Tanzania; Gore Mountain, NH, USA). Carbonate rocks altered by contact metamorphism that produced skarns contain garnet with compositions corresponding to mainly grossular (e.g., Sierra De Cruces, Coahuila, Mexico) or in some cases, andradite (e.g., Erongo Mountains, Namibia). Meta-ophiolitic rocks formed by the metasomatic alteration of peridotite and gabbroic protoliths contain uvarovite and grossular, respectively (Toulumne County, CA, USA; Outokumpu, Finland; Eden Mills, VT, USA; Jeffrey Mine, Quebec, Canada).

Metal sulfide-oxide-silicate ore deposits host two main garnet compositions depending on the origin of the host rocks. The Zn–Fe–Mn deposit of the Franklin Mine (NJ, USA) contains andraditic garnet as part of a skarn-like assemblage that includes calcite, magnetite and clinopyroxene produced through hydrothermal alteration of the host marble. Spessartine is genetically associated with garnetiferous units of the Pb–Zn–Ag deposit Broken Hill (New South Wales, Australia).

### 3.3. Previous LIBS Analysis of Garnet

In a study of 157 garnets from 92 localities worldwide that include some of the same garnets from this study Alvey et al. [24] demonstrated how LIBS analysis could be used to distinguish the six common garnet types. Because chemical analyses were not available, the museum collection or commercial label accompanying each sample was accepted as the garnet type classifications for that study. More recently, Harmon et al. [25] used LIBS analysis to differentiate between garnets from various geologic contexts, such as discriminating pyropes from different kimberlite localities in South Africa. Here we expand on these previous studies through comparative chemometric analysis of LIBS broadband spectra obtained by both a laboratory LIBS system and a handheld LIBS analyzer for 208 garnet specimens whose elemental composition was determined through electron microprobe (EMP) analysis.

## 4. Analytical Methods

### 4.1. Electron Microprobe Analysis

The quantitative chemical analysis of garnet by EMP analysis was performed in wavelength dispersive X-ray spectroscopy mode using a JEOL 8900 Superprobe electron microprobe at the Smithsonian Institution National Museum of Natural History. The

system was operated at an accelerating voltage of 15 kV, a beam current of 20 nA, a beam diameter of 1  $\mu\text{m}$  and counting times of 20 s on peaks and 10 s for backgrounds. Mineral standards used were Kakanui hornblende (K, Mg), ilmenite (Fe, Ti), grossular (Si, Al), manganite (Mn), apatite (Ca, P), and chromite (Cr). A conventional ZAF routine was used for data reduction. Representative microprobe analyses for the six near-end member compositions, whose LIBS spectra are displayed in Figure 1, are shown in Table 1.

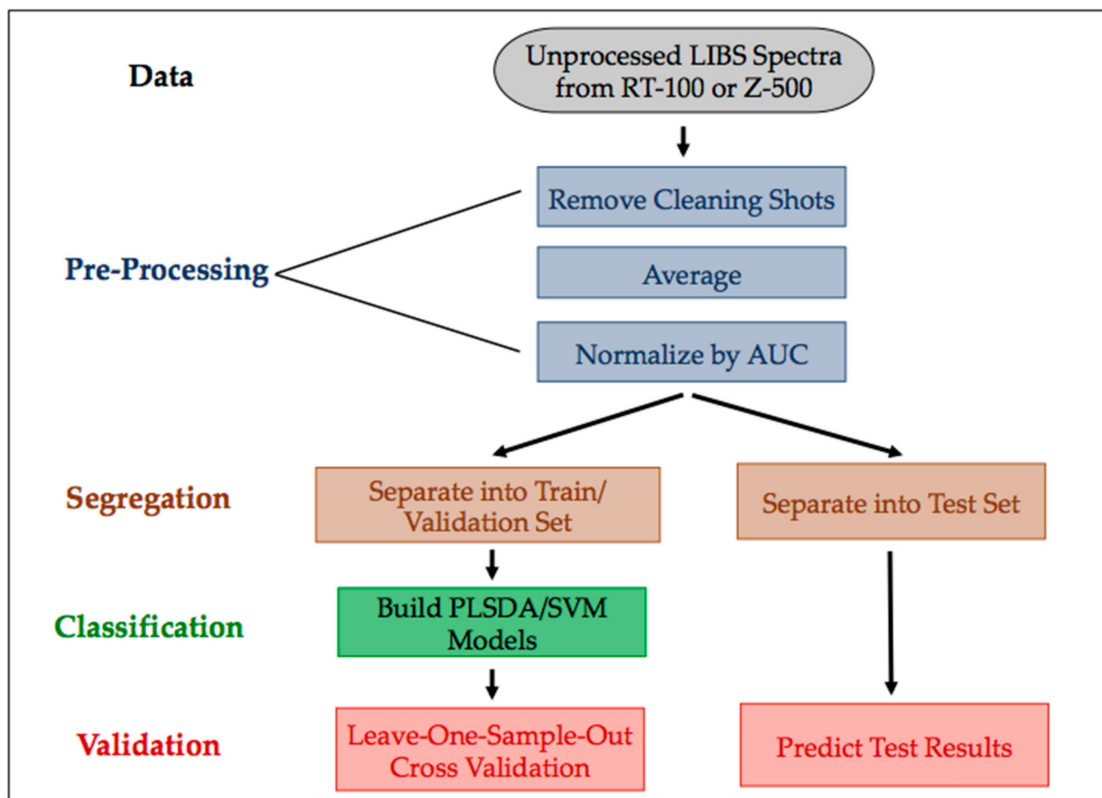


Figure 1. Spectral processing and chemometric procedure flow diagram for this study.

Table 1. Examples of electron microprobe analyses (reported as oxide wt %) for near end-member compositions of the six common garnet types, whose broadband LIBS spectra are displayed in Figures 2 and 3.

Sample ID	Labeled Type	MgO	FeO	MnO	CaO	ZnO	Al <sub>2</sub> O <sub>3</sub>	Cr <sub>2</sub> O <sub>3</sub>	SiO <sub>2</sub>	TiO <sub>2</sub>	K <sub>2</sub> O	P <sub>2</sub> O <sub>5</sub>	Total	Assigned Type
B19430	almandine	0.76	40.67	0.68	1.03	0.03	21.32	0.02	34.17	0.28	<0.01	0.02	98.98	almandine
R3418	pyrope	20.64	8.01	0.32	4.28	0.01	21.58	2.67	43.50	0.41	<0.01	0.01	101.43	pyrope
30	spessartine	0.02	2.34	40.69	0.18	0.07	21.16	0.01	35.20	0.02	<0.01	0.15	99.86	spessartine
R11362	grossular	0.02	0.61	0.63	36.74	0.05	22.36	0.20	38.83	0.10	<0.01	0.02	99.56	grossular
64	andradite	0.08	30.00	0.03	33.70	0.02	0.34	0.00	35.22	0.03	<0.01	0.01	99.43	andradite
161032	uvarovite	0.42	0.54	0.66	33.48	0.15	7.91	19.07	36.46	0.19	<0.01	0.02	98.76	uvarovite

#### 4.2. LIBS Analysis

Two LIBS systems were utilized for this study, a RT-100 commercial laboratory system (Applied Spectra, Inc., West Sacramento, CA, USA) and the Z-500 handheld LIBS analyzer (SciAps, Inc., Woburn, MA, USA). Both the RT-100 and Z-500 analyses were undertaken in the LIBS laboratory of co-author RRH at Juniata College. Data from the laboratory LIBS system was included in this study to provide a comparison with the handheld LIBS unit and confirm that both instruments provide similar results.

The RT-100 (Applied Spectra, Inc.) is a versatile laboratory LIBS system that comprised of a 50-mJ Nd:YAG laser operating at 1064 nm with a 5-ns pulse width and 1–20-Hz variable repetition rate, and six gated Czerny–Turner spectrographs coupled with high-

performance charge-coupled diode (CCD) detectors to provide coverage from 187–1044 nm at a resolution of 0.055–0.068 nm. This configuration produces composite LIBS spectra consisting of approximately 12,284 data points. User controlled operational parameters include laser power, signal acquisition delay time, and gate width. Operational parameters that can be controlled include laser power, gate width, and signal acquisition delay time. The RT-100 has an automated 3D translational stage that permits data to be collected over a user-defined grid pattern at 0.5-mm spacing, with a guide laser for ablation spot location, complementary metal–oxide–semiconductor (CMOS) camera imaging, and active focusing system that automatically refocuses the laser onto the surface each time the stage is moved to a new surface location. The RT-100 instrument collected 110 total spectra from a single location on each sample. The first two spectra were removed as ‘cleaning shots’, and the remaining 108 were averaged in groups of 18 for a total of 6 averaged spectra per sample.

Handheld LIBS analyzers are well suited to geochemical applications particularly for real-time analysis outside a traditional laboratory setting or in the field during geological fieldwork due to its portability and versatility. The work reported here utilized a Z-500 (SciAps, Inc.) handheld LIBS analyzer that employs a 1064 nm Nd:YAG pulsed laser with 50  $\mu\text{m}$  focused beam size that delivers 6 mJ to the sample with a 1 ns pulse duration at a firing rate between 1–10 Hz. The instrument can operate in the ambient atmosphere, but also is capable of gas purging that delivers an inert gas (He or Ar) directly to the focusing area on the sample surface where the LIBS plasma formation occurs for signal enhancement. The analyzer records a broad range of plasma light emission from 180–675 nm. Typical detection limits are in the tens to hundreds of ppm range for most elements when averaged across 2 mm<sup>2</sup> area of sample collection points, which is possible with its rastering capability. The LIBS emission signal is collected, and the light passed by fiber optic cable into four internal spectrometers with spectral ranges of 180–254, 254–314, 314–423 and 423–675 nm that use time-gated CCD detectors with resolution of 0.1 nm full width at half maximum (FWHM) below 423 nm and 0.3 nm FWHM above 423 nm. This produces composite LIBS spectra consisting of approximately 14,850 data points. Regular spectrometer wavelength calibration is performed by interrogation of an internal target made from Grade 316 Mo-bearing stainless steel. For each spectrometer in the unit, wavelength errors between selected observed emission lines and the values found in the National Institute of Standards and Technology (NIST) Atomic Spectra Database [26] are determined and correction coefficients are applied. These new coefficients are used until the next wavelength calibration is performed, with a record kept of all calibration spectra and correction values. The data for this study was collected with a 646 ns delay time, although the instrument is capable of variable gate delays from 250 ns up to 100  $\mu\text{s}$  in 20.8 ns increments. With the Z-500, six locations were analyzed for each sample. After three cleaning shots, five recorded spectra were averaged to a single spectrum per location resulting in a total of six averaged spectra. The data collection parameters for both the RT-100 and Z-500 represented typical settings used for routine analysis and are not the result of focused parameter optimization efforts.

There is inherent pulse-to-pulse variability in the energy distribution within pulses generated by the nanosecond lasers used in LIBS instruments. Even with an absolutely homogeneous sample, this leads to small differences in emission intensity from one measurement to the next that results in an intrinsic degree of measurement imprecision. Therefore, to improve data quality for this study, multiple laser shots were made at each analysis location on a sample and each broadband spectrum collected was intensity normalized. Additionally, non-analytical surface cleaning shots were performed prior to the collection of data with the handheld analyzer.

#### 4.3. Comparison of Sample Preparation and Analysis Time for EMP and LIBS

Preparation of samples for microprobe analyses is time-consuming and tedious. Fragments and crystals of garnet were selected, and hand separated from rock samples. Large pieces of garnet were broken into fragments 2–4 mm in width and mounted in holes

pre-drilled into Bakelite slabs. In general, nearly 8 h were needed to select and extract 25 garnet samples from their host rock with an additional hour needed to load the samples into a single Bakelite slab. The process of filling the holes with epoxy, allowing the epoxy to cure, and polishing the mount to yield a flat and uniformly smooth surface generally took 3–4 h to complete. Prior to the EMP analysis, garnet mounts must be coated by a thin layer of carbon, to reduce charge buildup and heating in the nonconductive garnet. It takes an automated coater nearly 10 min to apply the carbon coat simultaneously to two probe mounts. Data collection by EMP analysis utilizes an automated program for each spot analysis. Five analyses were collected across each garnet grain, with each analysis requiring approximately 8 min to complete.

By comparison, minimal sample preparation is required for LIBS analysis by the laboratory system, other than obtaining a sample of requisite size mounted in an appropriate manner, whereas no sample preparation is required for handheld analysis. Since each analysis with the handheld instrument is completed in less than 5 s, LIBS analysis is more than two orders of magnitude more rapid than EMP analysis. In the museum collection example of interest here, where a mineral collection is contained in multi-drawer cabinets, less than a minute is required for the compositional analysis of a single garnet specimen by handheld LIBS, so that more than 400 samples could be analyzed during a typical 8-h workday.

#### 4.4. Chemometric Analysis

The application of mathematical and statistical calculations to complex multivariate data, particularly spectroscopic data, as a means of extracting information that is not intuitive or obvious from simple bivariate or trivariate plots, is termed chemometric analysis [27]. Our data handling procedure for this study is illustrated schematically in Figure 1. Data for chemometric analysis took the form of LIBS broadband spectra as illustrated in Figures 2–4. Chemometric analysis was performed in Python (Version 3.8) using a bespoke code written by the first author that is available upon request. For chemometric analysis, both sets of LIBS spectra were processed following intensity normalization and spectral averaging [28]. Each averaged spectrum is divided by its respective integrated area under the curve (AUC), so that the chemometric classification was not based simply on overall peak magnitude. Principal component analysis (PCA) was used to condense the data into a representation of several combined features for visualization that best capture the meaningful differences in sample composition [29]. Our chemometric analysis utilized two statistical approaches—partial least squares discriminant analysis (PLSDA) and linear support vector machine classification (SVM).

Data for each classification task was split between training and testing sets. The dataset for the ‘garnet type’ classification task contained the 172 training samples whose labels were correct based on EMP analysis, whereas the 36 test samples were those samples in the two garnet collections documented as being incorrectly labeled or lacking labels. A range of hyperparameters were tested for each classifier, and the condition with the best overall accuracy was selected as the representative result. The number of latent variables was varied between 1–30 for PLSDA, and the value of ‘C’ was varied at intervals between 0.1 and 500 for SVM (i.e., 0.1, 0.3, 0.5, 0.6, 0.7, 0.8, 0.9, 1, 3, 5, 7, 10, 20, 50, 70, 100, 150, 250, 500). The choice of regularization parameter influences the precision/recall tradeoff for each model. Classification matrices were output at each hyperparameter condition, describing the classification accuracy for the training and test sets. The training set classification matrices were evaluated with grouped ‘leave-one-sample-out’ cross validation. Here, all spectra of a single sample were removed and tested against the remaining training data. This process was repeated for all samples, and the results were averaged. The test set classification matrices were evaluated by comparing the predicted versus actual classes of the test data against the model constructed from all the training data.

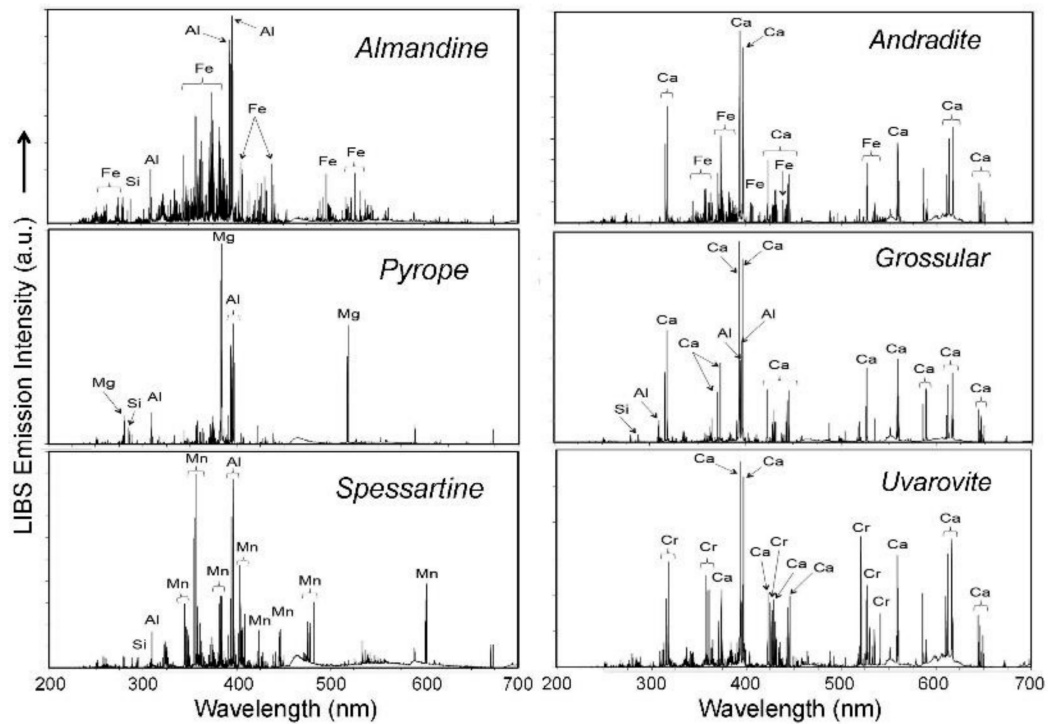


**Figure 2.** Examples of unprocessed broadband spectra between 200–700 nm acquired from averaging five laser shots by a RT-100 laboratory LIBS system for almandine B19430, pyrope R3418, spessartine 30, andradite 64, grossular R11362, and uvarovite 161032, which are near end-member compositions (Table 1).

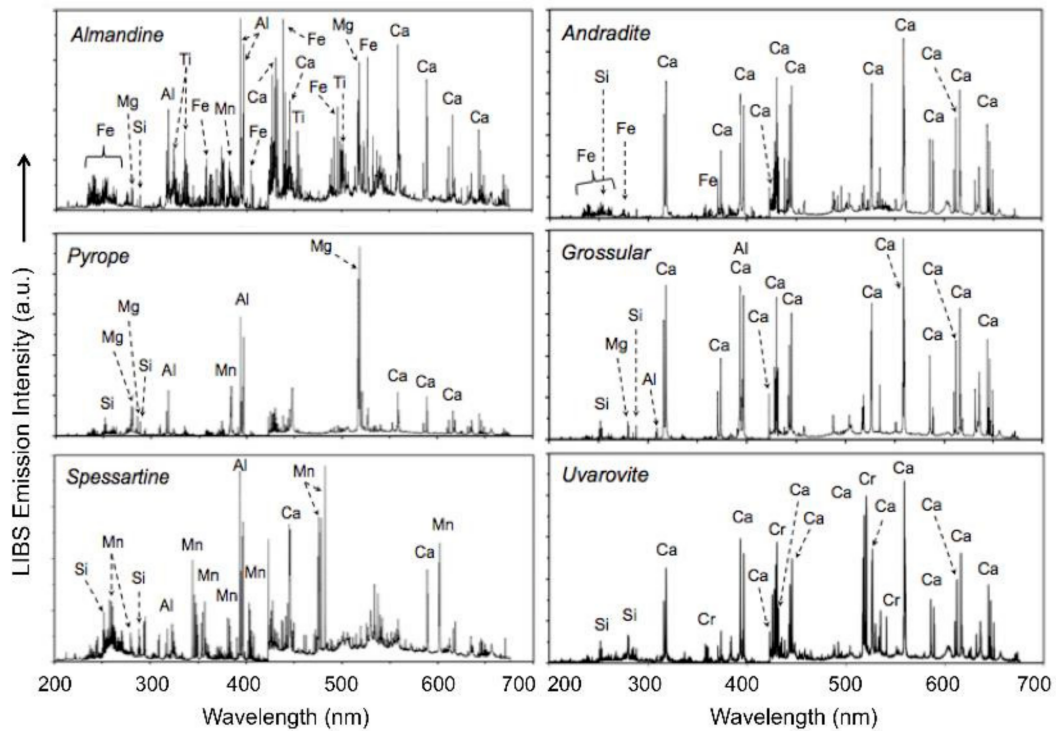


**Figure 3.** Example of unprocessed broadband spectra between 200–700 nm acquired from averaging five laser shots by a Z-500 handheld LIBS analyzer for almandine B19430, pyrope R3418, spessartine 30, andradite 64, grossular R11362, and uvarovite 161032, which are near end-member compositions (Table 1).



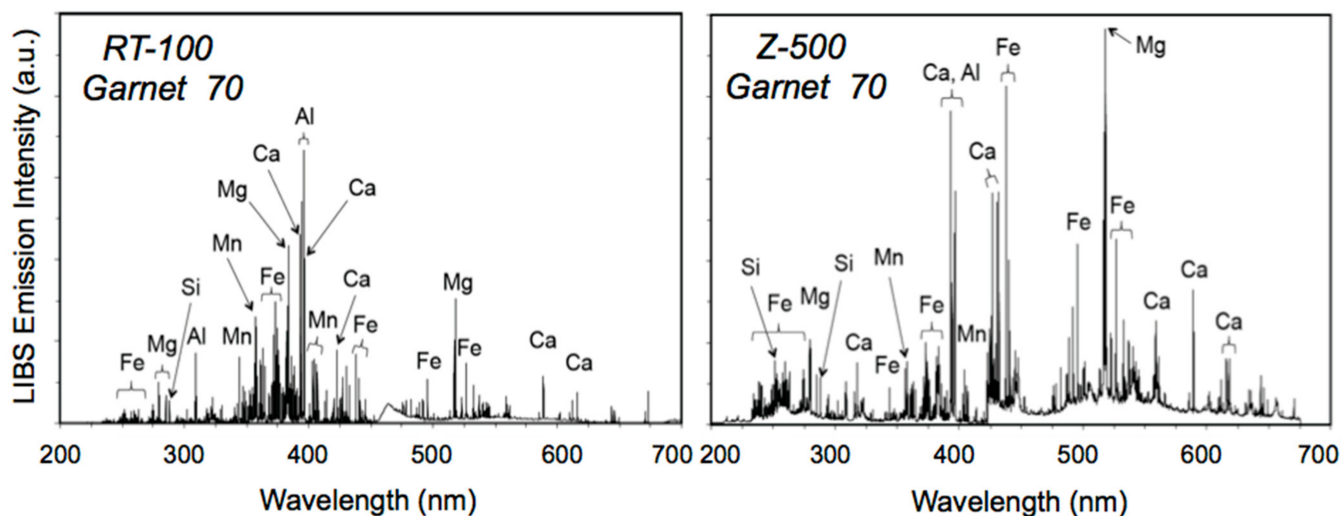


**Figure 4.** Comparison of unprocessed RT-100 (left) and Z-500 (right) broadband LIBS spectra for sample 70, a mixed composition garnet labeled as a grossular with 4.87% MgO, 30.20% FeO, 1.23% CaO, 3.69% MnO, and 22.03% Al<sub>2</sub>O<sub>3</sub> that was reclassified as an andradite on the basis of EMP analysis.

## 5. Results and Discussion

### 5.1. Garnet Composition

Garnet composition is highly variable and mainly depends on bulk-rock geochemistry, together with the pressure, and temperature conditions under which the garnet crystallized. Species designation of an individual garnet is based on the dominant cation that occupies the dodecahedral X, octahedral Y, and tetrahedral Z crystallographic sites of the garnet structure [30,31]. Conventionally, the named garnet species relies on determining the proportion of garnet end-member components which are typically calculated from chemical analyses. Though all garnets have a readily recognizable dodecahedral form, each type can display a wide range of colors because of their intrinsically complex chemistry, so it is not possible to be certain of a type assignment for a garnet without knowledge of its composition. Hence, we undertook EMP analysis of our 208 samples to ascertain the extent to which the assigned labels of these specimens were in fact correct. Respective ranges of dominant cation contents measured for the six garnet types were:

Almandine	FeO = 40.67–21.37 wt % and Al <sub>2</sub> O <sub>3</sub> = 23.84–16.69 wt %,
Pyrope	MgO = 25.94–11.70 wt % and Al <sub>2</sub> O <sub>3</sub> = 24.35–23.72 wt %,
Spessartine	MnO = 42.37–16.87 wt % and Al <sub>2</sub> O <sub>3</sub> = 21.87–10.87 wt %,
Grossular	CaO = 37.31–25.12 wt % and Al <sub>2</sub> O <sub>3</sub> = 26.15–8.56 wt %,
Andradite	CaO = 35.15–20.41 wt % and FeO = 12.54–30.00 wt %,
Uvarovite	CaO = 34.92–33.48 wt % and Cr <sub>2</sub> O <sub>3</sub> = 19.07–15.31 wt %.

For garnets whose composition exhibit significant solid solution, Mn ranged up to 20.96 wt %, Mg up to 10.90 wt %, and CaO up to 7.87 wt % in some almandines; FeO ranged up to 20.86, MnO up to 20.74 wt %, and CaO to 7.56 wt % in some pyropes; FeO ranged up to 21.15 wt % and CaO up to 17.19 wt % in some spessartines; MnO ranged up to 12.42 wt %, MgO up to 11.92 wt %, and Al<sub>2</sub>O<sub>3</sub> up to 10.12 wt % in some andradites; FeO ranged up to 16.22 wt % in some grossulars; and FeO ranged up to 11.31 wt % and Al<sub>2</sub>O<sub>3</sub> to 7.92 wt % in some uvarovites. For this application, we applied the program of Locock [32] to recast the EMP analyses expressed as weight percent oxides into end-member garnet components based upon a calculation of the amounts of Fe<sup>2+</sup>, Fe<sup>3+</sup>, and Mn<sup>3+</sup>, by stoichiometric constraints. Other programs for calculating garnet components from chemical analyses [33,34] produced similar results. Representative examples of our microprobe analyses for each garnet type are given in Table 1.

### 5.1.1. Comparison of RT-100 and Z-500 LIBS Analysis

Typical broadband spectra obtained by the RT-100 laboratory LIBS system and the Z-500 handheld LIBS analyzer for near end-member compositions of the six common garnet types (Table 1) are displayed in Figures 2 and 3, with predominant emission lines identified in both figures. Figure 4 presents a side-by-side comparison of spectra for grossular 70. Over the 200–700 spectral range shown in these figures, the element Si is identified by a few well-defined spectral lines, Al, Mg, and Ca by a larger number of discrete lines or pairs of lines, and Fe, Mn, and Cr by sets of multiple adjacent lines. In these figures, the RT-100 and Z-500 spectra for each of the six garnet types are dominated by the expected element pairs—Fe–Al for almandine, Mg–Al for pyrope, Mn–Al for spessartine, Ca–Fe for andradite, Ca–Al for grossular and Ca–Cr for uvarovite, but it is notable that there are distinct differences in the pair of spectra for each garnet type.

The RT-100 laboratory system covers a broader wavelength range (180–1040 nm) and employs a laser with nearly ten times the power of the handheld unit (50 mJ versus 6 mJ, respectively). By contrast, the Z-500 has a smaller wavelength range (180–675 nm) but better spectral resolution and utilizes an Ar gas purge during analysis to increase the intensity of the spectral lines. LIBS plasma emissions were collected using slightly different gate delay times, 1 ms for the RT-100 compared to 646 ns for the Z-500, which is responsible for further differences in the intensity of lines across the spectral range of signal acquisition. Additionally, the two LIBS instruments do not have the same sensitivity over all portions of the spectral range. For example, the Si peaks at 251.6 and 288.2 nm are significantly lower in intensity, or even not detected, in the RT-100 spectra compared to the Z-500 spectra (Figures 2–4), demonstrating that the laboratory instrument has diminished capability in the ultraviolet region due either to reduced transmissivity of the signal through the optical components of the system or an attenuated sensitivity of the spectrometer channels in this wavelength area. By contrast, the RT-100 is more sensitive in the spectral range between 400–600 nm where Fe and Mg emission lines are more intense than in the Z-500 spectra.

As documented in Tables 2 and 3, some of the samples in our collections had been misidentified—27 of the 151 samples (i.e., 17.8%) in the NMNH collection and 10 of the 54 (i.e., 18.5%) in the personal collection. The most common misclassifications were six instances each of almandine labeled as spessartine and grossular labeled as andradite followed by five instances spessartine labeled as almandine. Three andradites were labeled as grossular. Other labeling misclassifications with one or two instances each were almandine as grossular or pyrope, andradite as almandine or uvarovite, grossular as uvarovite, pyrope as andradite, and spessartine as andradite, grossular or pyrope. Two of the three samples labeled as hydrogrossular  $[\text{Ca}_3\text{Al}_2(\text{SiO}_4)_{3-x}(\text{OH})_{4x}]$  were grossular and the other was an andradite, the three samples labeled as schorlomite  $[\text{Ca}_3(\text{Fe}^{3+}, \text{Ti})_2(\text{Si}, \text{Ti})_3\text{O}_{12}]$  were actually andradite, and a sample labeled as calderite  $[(\text{Mn}^{2+}, \text{Ca})_3(\text{Fe}^{3+}, \text{Al})_2(\text{SiO}_4)_3]$  was grossular. The 37 mislabeled samples were reclassified to their correct type based upon their microprobe analyses and the two samples with no prior type attribution were appropriately classified, so that the database for the chemometric analysis comprised 42 almandines, 40 andradites, 54 grossulars, 18 pyropes, 48 spessartines, and 6 uvarovites.

### 5.1.2. Garnet Discrimination by PCA

PCA was applied to the LIBS broadband spectra after the pre-processing described in Section 4.4 above to compare the extent of garnet type discrimination on the basis of the broadband LIBS spectra acquired by the RT-100 laboratory system and the Z-500 handheld analyzer, like those shown in Figures 1 and 2. PCA is an unsupervised matrix analysis technique that employs an orthogonal transformation to convert a set of observations of possibly correlated variables into a set of linear combinations of uncorrelated variables, termed principal components, that describe major compositional trends in an analytical data set [35]. This transformation is undertaken in such a way that the first principal component accounts for as much of the variability in the data set as possible, with each succeeding component in turn explaining the next greatest proportion of the residual

variance given the constraint that it is orthogonal to the preceding components. A score along each principal component can be calculated for every sample in the dataset and these can be plotted to show the compositional relationships between samples. The first few components generated by PCA typically account for the majority of the variance and, therefore, provide an adequate representation of the data for visualization purposes, with the results projected onto the first 2–3 principal components to visually portray the relative separation of the samples in each class. This type of exploratory data analysis provides a graphical representation of the natural grouping of the samples and highlights which variables (i.e., LIBS emission wavelengths in this study) most strongly influence the clustering. Thus, PCA provides a useful tool for both visualizing whether samples are similar or different and identifying which variables are responsible for observed similarities and differences, but is not, in general, an appropriate tool for classification of unknown data.

**Table 2.** Examples of electron microprobe analyses for correctly classified (1) and misclassified (2) garnets, based on the museum or collection label.

Sample ID	Labeled Type	MgO	FeO	MnO	CaO	ZnO	Al <sub>2</sub> O <sub>3</sub>	Cr <sub>2</sub> O <sub>3</sub>	SiO <sub>2</sub>	TiO <sub>2</sub>	K <sub>2</sub> O	P <sub>2</sub> O <sub>5</sub>	Total	EMP Assigned Type
<b>1. Examples of Correct Classifications</b>														
68	almandine	1.10	40.12	0.44	0.36	0.02	21.29	0.01	34.44	0.06	<0.01	0.10	97.92	almandine
B19430	almandine	0.76	40.67	0.68	1.03	0.03	21.32	0.02	34.17	0.28	<0.01	0.02	98.98	almandine
64	andradite	0.08	30.00	0.03	33.70	0.02	0.34	0.00	35.22	0.03	<0.01	0.01	99.43	andradite
171064	andradite	0.03	26.70	0.22	29.85	0.03	1.76	0.01	37.04	0.19	<0.01	0.02	95.83	andradite
27	grossular	0.77	2.54	0.12	36.16	0.01	20.91	<0.01	39.08	0.13	<0.01	0.01	99.75	grossular
139717	grossular	0.02	0.66	0.63	36.54	0.04	21.83	0.75	38.72	0.03	0.01	0.01	99.23	grossular
122845	pyrope	19.72	8.96	0.24	4.33	<0.01	24.35	0.27	43.56	0.13	0.01	0.04	101.59	pyrope
R3418	pyrope	20.64	8.01	0.32	4.28	0.01	21.58	2.67	43.50	0.41	<0.01	0.01	101.43	pyrope
135296	spessartine	<0.01	0.72	42.13	1.31	0.01	21.36	0.01	32.60	0.09	<0.01	0.01	98.53	spessartine
48745	spessartine	<0.01	1.93	40.81	0.82	0.02	21.33	0.01	35.35	0.05	<0.01	0.01	100.51	spessartine
62	uvarovite	0.03	0.47	0.04	34.92	0.02	7.45	18.88	35.67	0.77	<0.01	0.01	98.25	uvarovite
123380	uvarovite	0.41	0.57	0.69	33.69	<0.01	8.12	18.86	35.56	0.08	<0.01	0.03	97.99	uvarovite
<b>2. Examples of Misclassifications</b>														
118214	almandine	0.27	17.32	24.45	1.51	0.05	20.78	<0.01	34.94	0.10	<0.01	0.02	99.47	spessartine
69	andradite	0.58	7.88	0.06	36.22	<0.01	15.95	0.21	38.54	0.38	<0.01	0.02	99.87	grossular
75	andradite	16.73	14.37	0.36	3.77	0.02	24.11	0.03	42.83	0.04	<0.01	0.01	102.26	pyrope
R3469	andradite	0.17	13.51	15.76	18.40	0.40	10.87	<0.01	36.32	0.04	<0.01	<0.01	95.45	spessartine
123378	grossular	0.02	16.90	0.23	35.15	<0.01	10.12	<0.01	36.71	0.13	<0.01	0.01	99.26	andradite
143894	pyrope	10.90	24.55	1.52	1.70	0.02	23.34	0.04	40.98	0.01	0.01	<0.01	103.15	almandine
R16774	spessartine	0.08	24.59	18.11	0.14	0.03	21.13	<0.01	36.13	0.08	<0.01	0.15	100.44	almandine
107314	uvarovite	0.05	19.20	0.06	34.00	0.05	0.74	9.58	35.42	0.18	<0.01	<0.01	99.28	andradite
26	uvarovite	0.10	11.27	0.04	34.07	0.02	0.84	16.63	34.83	1.14	<0.01	0.02	98.96	grossular

**Table 3.** Examples of electron microprobe analyses and type assignments for correctly classified (left) and misclassified (right) garnets.

Sample ID	Correctly Labeled						Incorrectly Labeled					
	68	171064	27	122845	135296	62	118214	69	123378	143894	R16774	107314
labeled type	almandine	andradite	grossular	pyrope	spessartine	uvarovite	almandine	andradite	grossular	pyrope	spessartine	uvarovite
MgO	1.10	0.03	0.77	19.72	<0.01	0.03	0.27	0.58	0.02	10.99	0.08	0.05
FeO	40.12	26.70	2.54	8.96	0.72	0.47	17.32	7.88	16.90	24.55	24.59	19.20
MnO	0.44	0.22	0.12	0.24	42.13	0.04	24.45	0.06	0.23	1.52	18.11	0.06
CaO	0.36	29.85	36.16	4.33	1.31	34.92	1.51	36.22	35.15	1.70	0.14	34.00
Al <sub>2</sub> O <sub>3</sub>	21.29	1.76	20.91	24.35	21.36	7.45	20.78	15.95	10.12	23.34	21.13	0.74
Cr <sub>2</sub> O <sub>3</sub>	0.01	0.01	<0.01	0.27	0.01	18.88	<0.01	0.21	<0.01	0.04	<0.01	9.58
SiO <sub>2</sub>	34.44	37.04	39.08	43.56	32.60	35.67	34.94	38.54	36.71	40.98	36.13	35.42
<b>End-Member %</b>						<b>End-Member %</b>						
Grossular			88.08%	10.07%	1.43%	31.73%		69.66%	43.01%	4.36%		
Andradite		73.99%				1.60%	0.42%	25.32%	53.93%			33.77%
Uvarovite						61.02%		0.65%				26.34%
Spessartine	1.04%	0.53%		0.47%	89.96%		57.09%			3.17%		
Almandine	89.63%	8.20%		17.48%			33.91%			50.48%	42.03%	
Pyrope		0.11%		68.58%						39.95%	56.35%	
EMP assigned type	almandine	andradite	grossular	pyrope	spessartine	uvarovite	spessartine	grossular	andradite	almandine	almandine	grossular

PCA plots for our RT-100 and Z-500 analyses are shown in Figure 5. For the RT-100 data set, the three principal components respectively account for 51.2%, 15.2%, and 14.2% of the variance in the data set, compared to 61.0%, 18.5%, and 5.1% for the Z-500 data set.

Both data sets exhibit good compositional differentiation. In both cases, the six garnet types are differentiated by three vectors denoting the solid solution of divalent cations in the dodecahedral X structural site and octahedral trivalent cations in Y structural site that have different geometric orientations in the PCA plots. Grossular, andradite, and uvarovite are differentiated along a  $\text{Fe}^{3+}$ -Al-Cr vector, spessartine is separated from almandine along a  $\text{Fe}^{2+}$ -Mn vector, and pyrope distinguished from almandine along a  $\text{Fe}^{2+}$ -Mg vector. Thus, we can conclude that LIBS analysis is effective in discriminating the six common garnet species based on their major element composition.

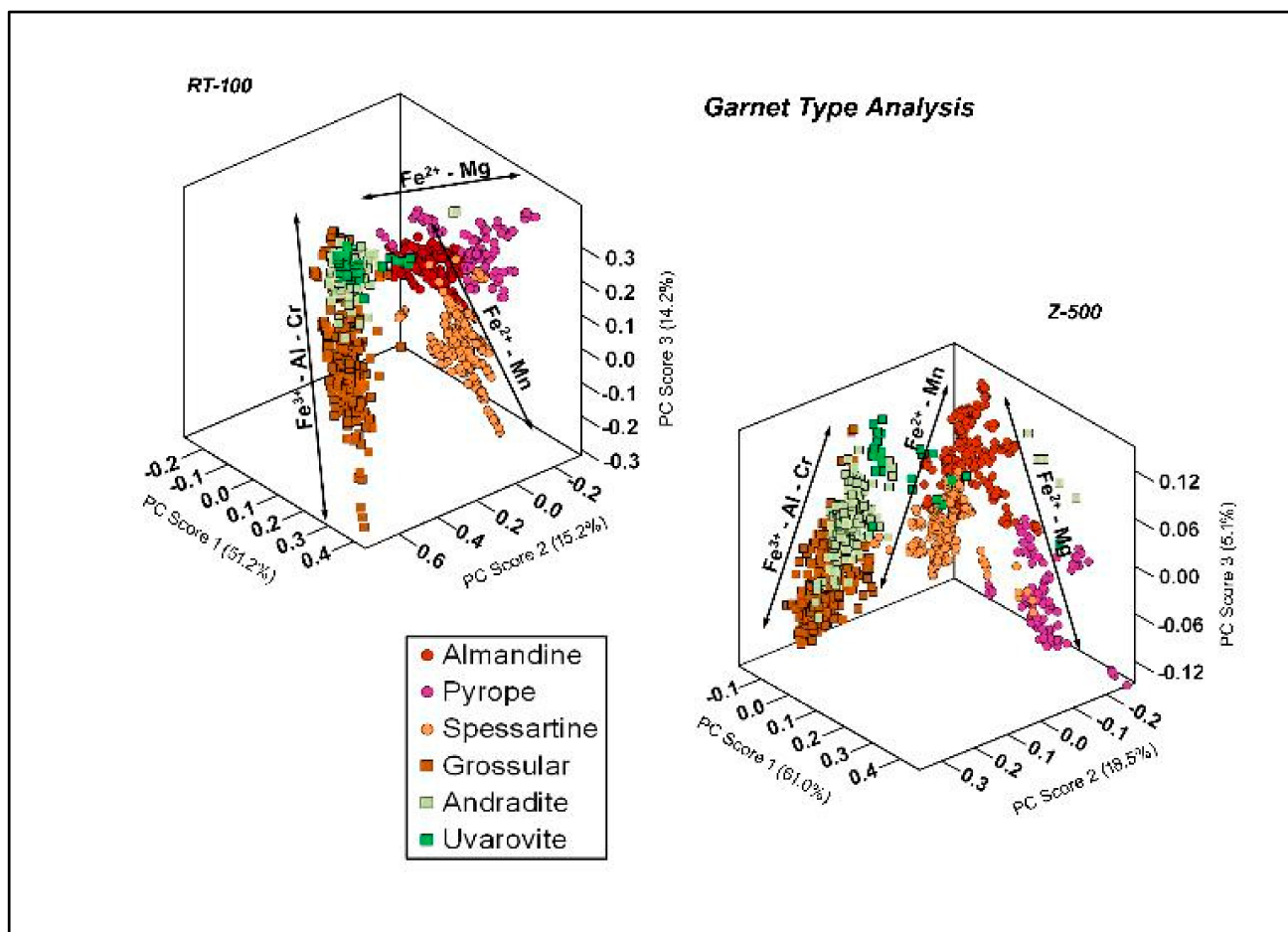


**Figure 5.** PCA scores plots for processed LIBS broadband spectra for the training set of 172 garnets (31 almandines, 33 andradites, 46 grossulars, 17 pyropes, 39 spessartines, and 6 uvarovites) acquired with the RT-100 laboratory system (**upper left**) and Z-500 handheld analyzer (**lower right**) showing respective  $\text{Fe}^{3+}$ -Al-Cr,  $\text{Fe}^{2+}$ -Mn, and  $\text{Fe}^{2+}$ -Mg trends.

### 5.1.3. Comparison of PLSDA and SVM Chemometric Analysis

PLSDA is a supervised pattern recognition and classification technique based on principal components and ordinary multiple regression analysis that builds a linear model based upon input data with labels to train a classifier, the performance of which is then tested by inputting additional data to assess the accuracy of the output data labels [35–38]. PLSDA searches for a subspace by which to project independent variables (samples) onto dependent variables (class labels) such that the covariance between the independent and dependent variables is maximized. This creates a model for transforming additional samples into estimates of class labels. The PLSDA model employed here used leave-one-sample-out cross validation.

SVM is a suite of related supervised learning methods based on generalized linear regression that can be used for classification in high-dimensional space [39]. By comparison

to other machine learning methods that are based on minimizing empirical risk, SVM is designed to minimize structural risk through finding the ideal compromise between learning capability with minimum information and accuracy of the algorithm. SVM maps input vectors into a high dimensional space, where a hyperplane of maximum separation is derived from parallel hyperplanes constructed on each side of the data. The separating hyperplane is that which maximizes the distance between the two parallel hyperplanes while simultaneously minimizing the empirical classification error and maximizing the geometric margin [40]. For classification problems, the assumption is made that the larger the margin or distance between these parallel hyperplanes, the better will be the performance of the classifier. Several recent studies have reported that the SVM method can result in better classification performance than other approaches when applied to LIBS spectral data for geological materials such as rocks and minerals [41–43].

The PLSDA and SVM results for the full garnet dataset are presented in Figure 6 and Figure 7 in the form of classification diagrams. These bivariate plots portray the reclassification of the observations determined by the two chemometric approaches from the LIBS spectra obtained by RT-100 and Z-500 for the training and testing analysis. Each entry in the classification matrix indicates the percentage of the LIBS spectra that were identified as belonging to the column class, when in fact they are actually members of the row class. These figures illustrate that spectral signatures from both the laboratory LIBS system and the handheld LIBS analyzer were sufficient to permit discrimination of these compositionally complex samples with a high degree of confidence.

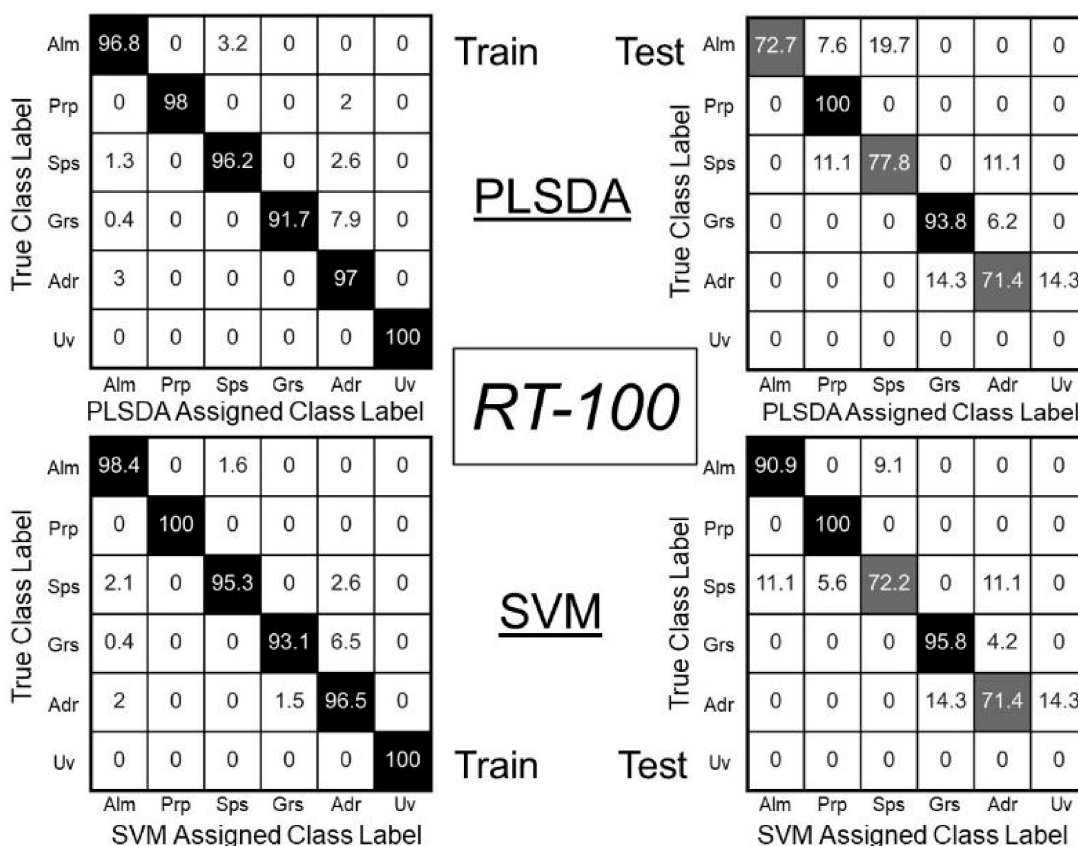


**Figure 6.** Classification diagrams for the training (left side) and testing (right side) sets for chemometric analysis of LIBS spectra obtained by the RT-100 laboratory LIBS system by PLSDA (top) and SVM (bottom). The classification accuracy of PLSDA and SVM for the training data was 95.5% and 96.1%, respectively, while corresponding values for the test data using PLSDA and SVM were 79.2% and 83.8%, respectively.

As illustrated in Figures 6 and 7, for both the RT-100 and Z-500 analyses, PLSDA and SVM performed extremely well for the training suite of 172 samples whose composition, discerned from EMP analysis, matched the assigned specimen label. It should be noted that the number of samples was not equally distributed among all garnet classes with pyropes and especially uvarovites being underrepresented compared to the other four types. The overall classification success rate for the RT-100 data was 95.5% for PLSDA and 96.1% for SVM, while the classification accuracy for the Z-500 data was slightly higher at 98.8% for PLSDA and 99.0% for SVM. For the RT-100 analyses, both algorithms achieved 100% classification success only for uvarovite, whereas 100% classification success was achieved for pyrope and spessartine for the Z-500 analyses. The fact that all training samples were not correctly classified and classified in a slightly different manner for the two data sets reflects both the extensive solid solution between the different garnet species and the aforementioned differences between the laboratory system and the handheld analyzer. Misclassifications, represented by off-diagonal entries in the training data diagrams, were generally of the same type and of the same approximate magnitude for the two instruments and both classifiers. For example, some spectra of almandine were misclassified as being spessartine at percentages that ranged from 1.6% to 3.2%, whereas some grossular spectra were misclassified as being either almandine at percentages of 0% to 0.4% or andradite at percentages of 0.4% to 7.9%.

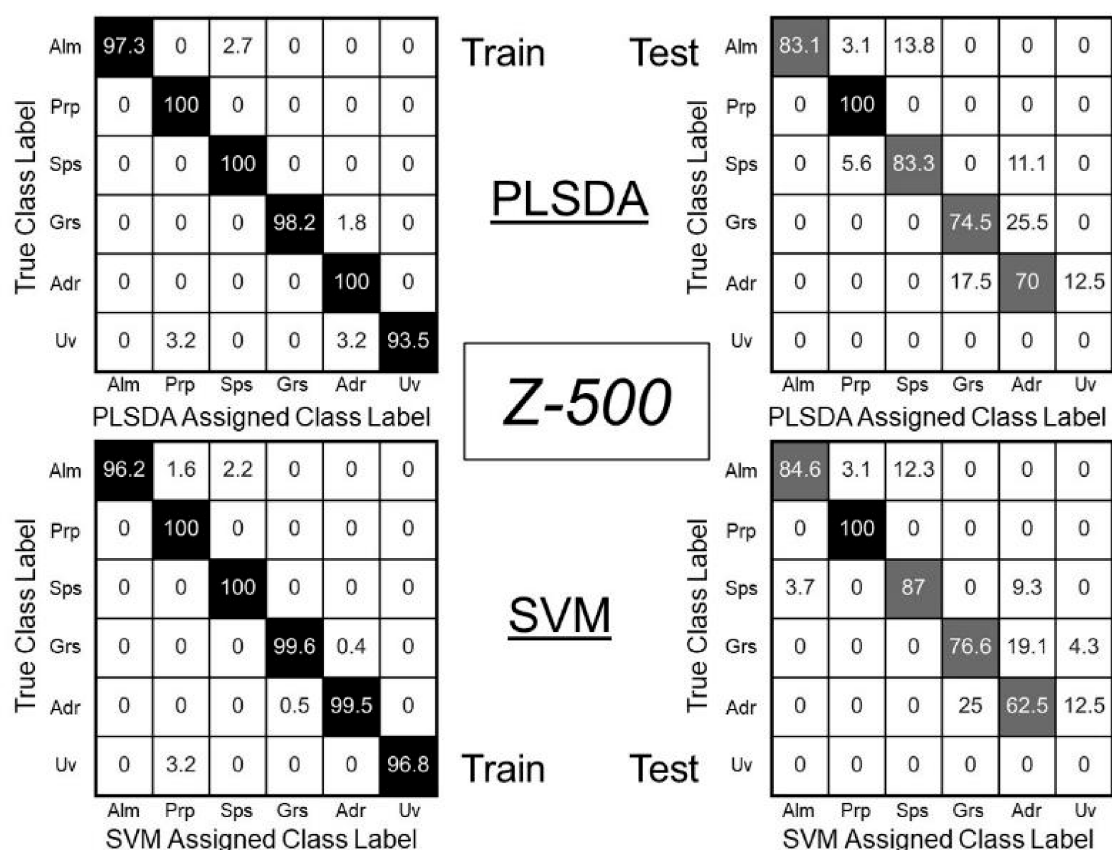


**Figure 7.** Classification diagrams for the training (left side) and testing (right side) sets for chemometric analysis of LIBS spectra obtained by the Z-500 handheld LIBS analyzer by PLSDA (top) and SVM (bottom). The classification accuracy of PLSDA and SVM for the training data was 98.8% and 99.0%, respectively, while corresponding values for the test data using PLSDA and SVM were 79.3% and 79.7%, respectively.

In order to evaluate the PLSDA and SVM classifiers with new data that had not been used to train the algorithms we selected specimens from the sample suite that were either mislabeled with the wrong garnet type (34 examples) or had no garnet assignment

on the label (2 examples). This included all the mislabeled samples shown in Table A1 (Appendix A) except for the two grossulars that were labeled as hydrogrossular and the three andradite samples that had been misidentified as schorlomite, all of which were used in the training set. The classification success for both the RT-100 and Z-500 analyses was significantly lower for the test samples that comprised the 36 mislabeled or unlabeled samples in the overall suite of 208 garnet specimens (Figures 6 and 7). It should be noted that there were no uvarovites in the group of test specimens. Admittedly, the selection criterion means that the test samples are not a randomly chosen subset of the larger sample suite, but instead those samples whose complex chemistry required EMP compositional analysis and did not permit correct type recognition by visual inspection alone. Therefore, it is not unexpected that the classification performance is diminished compared to the training data. The overall classification success rate for PLSDA of 79.2% was reduced relative to the 83.8% obtained with SVM for the RT-100 data. This compares to an equivalent performance for the Z-500 data of 79.3% for PLSDA and 79.7% for SVM. For the RT-100 analyses, both algorithms achieved 100% classification success only for the single pyrope sample, with the 8 grossulars and 11 almandines classified correctly at 93.8% and 72.7%, respectively, by PLSDA and both the grossulars and almandines classified successfully at >90% by SVM. The 9 spessartines and 7 andradites gave only modest correct classification results. The situation was similar for the Z-500 results with samples identified with the correct garnet class at levels less than 80%. Interestingly, the SVM algorithm, which had marginally outperformed PLSDA for both the training and testing sets of RT-100 and Z-500 data, was significantly surpassed by PLSDA for the andradites of the test set, achieving the lowest classification success of this study at just over 62%. The handheld and laboratory LIBS instruments achieved similar results using both classifiers, with the former slightly outperforming the latter with the training data. The situation was reversed with the test samples where the RT-100 did marginally better than the Z-500. However, since the difference in classification success is only a few percent it is safe to conclude that the portable unit performed on par with the much larger and more expensive laboratory instrument for this application.

One objective of this study was to demonstrate that handheld LIBS could be used in combination with machine learning tools to rapidly and efficiently carry out mineral analysis and specimen identification in a museum setting. In order to assess the reliability of the LIBS analysis, it is necessary to consider the potential limitations of this practical application. In addition to using classification diagrams to evaluate the efficacy of LIBS analysis for garnet discrimination, it is also possible to use a voting approach. Rather than using an aggregate percentage of correct or incorrect classifications, a voting approach tabulates the individual class assignment for each of the averaged spectra in the data set. Given the overall goal performing analysis on-site in a mineral collection storage room of a museum or in the field, our analysis is limited to the results obtained with the Z-500 handheld analyzer.

For this study, there were usually 6 averaged spectra for each of the 208 samples used for training and testing, i.e., a total of over 1240 class assignments, although in a few cases, only 5 average Z-500 spectra were collected. Table 4 shows only those samples for which all votes for either PLSDA or SVM were not to the correct garnet type, even if most votes were for the correct class. The two classifiers returned a nearly identical total number of 'wrong votes' (70 for PLSDA and 68 for SVM), though they differed in which samples had the misclassifications. In some instances, PLSDA correctly assigned all the votes to the correct class and SVM got every assignment incorrect (e.g., entries 14 and 20), whereas the situation was exactly reversed for other samples (e.g., entry 3). Based on a 'most votes' approach, PLSDA and SVM had 12 and 11 incorrect assignments, respectively, for an overall misclassification rate of less than 6% for both classifiers. A subset of the errors is attributable to the mixed compositional character of these garnets, as observed from the EMP analysis. For example, the end-member percentages for entries 1 and 13 differ less than 1%, so it is not surprising that PLSDA split the votes between the garnet

types with the two highest percentages. Interestingly, SVM correctly assigned the samples in both instances. However, entry 18 shows that both classifiers can be totally wrong when the end-member compositions are very close. Even in instances where there is a relatively large difference between the highest and next highest percentages, the assignments also can be incorrect, especially if the sum of the end-member percentages is significantly less than 100% (e.g., entries 5, 6 and 9). The sample suite was not studied with optical microscopy to visually determine the extent to which individual samples displayed zoning, but it would obviously be challenging to assign a specimen to a single garnet class if it were heterogeneous. Since the LIBS and EMP analyses were undertaken on the same samples but not necessarily the same locations, additional differences could arise, especially for non-homogeneous specimens. Having a larger number of samples with known chemistry might improve classification success but improvement could be minimal given the natural variety of garnets that can range from near end-member compositions to highly complex solid solutions.

**Table 4.** Summary of voting approach for classification of garnet specimens based on chemometric analysis of spectral data obtained by the Z-500 handheld LIBS analyzer using PLSDA and SVM. Only samples for which all votes for either PLSDA or SVM are not to the correct garnet type are shown. The remaining 187 samples from the training and test sets had all spectra classified correctly. The microprobe end-member analysis percentages are included for comparison. Sample identification numbers indicate whether the result is from the training or testing results (bold).

Entry #	Sample ID	Technique	Garnet Class					
			Grossular	Andradite	Uvarovite	Spessartine	Almandine	Pyrope
1	RH-29	Microprobe	<b>32.14%</b>	31.67%		0.33%	8.35%	
		Z-500 PLSDA	3	3				
		Z-500 SVM	1	5				
2	NMNH 47358	Microprobe	<b>65.82%</b>	7.87%		1.94%		
		Z-500 PLSDA	4	2				
		Z-500 SVM	5	1				
3	RH-26	Microprobe	<b>90.49%</b>	1.76%	1.76%			
		Z-500 PLSDA			5			
		Z-500 SVM	5					
4	NMNH 168752	Microprobe	<b>49.56%</b>	43.68%				
		Z-500 PLSDA		6				
		Z-500 SVM	1	5				
5	NMNH 16321	Microprobe	<b>46.04%</b>	15.55%		0.99%		
		Z-500 PLSDA		6				
		Z-500 SVM		6				
6	NMNH B19516	Microprobe	29.33%	<b>34.69%</b>		2.88%	8.88%	1.12%
		Z-500 PLSDA		6				
		Z-500 SVM	4	2				
7	NMNH 124835	Microprobe	32.85%	<b>41.98%</b>		1.77%		
		Z-500 PLSDA	1	5				
		Z-500 SVM		6				
8	RH-48	Microprobe	38.52%	<b>46.03%</b>		0.65%	5.54%	
		Z-500 PLSDA	4	2				
		Z-500 SVM	5	1				
9	NMNH 107314	Microprobe		<b>33.77%</b>	26.34%			
		Z-500 PLSDA			2		1	2
		Z-500 SVM			5			
10	NMNH 123378	Microprobe	43.01%	<b>53.93%</b>				
		Z-500 PLSDA	5	1				
		Z-500 SVM	6					
11	NMNH C5704	Microprobe		33.38%	51.10%			
		Z-500 PLSDA		1	5			
		Z-500 SVM			6			



Table 4. Cont.

Entry #	Sample ID	Technique	Garnet Class						
			Grossular	Andradite	Uvarovite	Spessartine	Almandine	Pyrope	
12	NMNH 161032	Microprobe Z-500 PLSDA Z-500 SVM	34.23%	1.04%	61.21%				1 1
13	RH-83	Microprobe Z-500 PLSDA Z-500 SVM	2.05%			43.30%	9.11%		42.95% 3
14	NMNH 166063	Microprobe Z-500 PLSDA Z-500 SVM				45.38%	40.27%		
15	NMNH R3469	Microprobe Z-500 PLSDA Z-500 SVM	7.21%	35.89%		40.75%			
16	NMNH 90518	Microprobe Z-500 PLSDA Z-500 SVM				1.91%	52.89%		
17	NMNH 166064	Microprobe Z-500 PLSDA Z-500 SVM				42.35%	42.73%		
18	RH-66	Microprobe Z-500 PLSDA Z-500 SVM	0.44%			47.30%	49.62%		0.33%
19	NMNH C5331-1	Microprobe Z-500 PLSDA Z-500 SVM				44.93%	52.02%		
20	NMNH C5331-2	Microprobe Z-500 PLSDA Z-500 SVM				47.16%	50.52%		
21	NMNH 143894	Microprobe Z-500 PLSDA Z-500 SVM	4.36%			3.17%	50.48%		39.95% 2

The results of this study suggest that one practical way to minimize the number of incorrectly labeled samples while taking advantage of the high throughput capacity of the LIBS technique would be to utilize two or more classifiers and adopt an ‘all votes’ approach for label assignments. This would entail using the LIBS method to rapidly analyze a large sample suite, carry out preprocessing and chemometric analysis with PLSDA and SVM, and then assign a label only if all the votes for both classifiers are for the same class. The ability of one classifier to mitigate the errors of second classifier argues for the use of more than one tool to reduce errors. Additional classification tools could also be explored to ascertain if better results can be achieved. In cases where there is not voting unanimity, those samples should be examined for quantitative compositional analysis. If this metric were applied to the present study, there are only two samples (Table 4, entries 5 and 18) that would have been incorrectly assigned as false positives with an additional 19 samples requiring further analysis. These results suggest that a hybrid LIBS/EMP approach would provide approximately 99% correct labels, which is a significant improvement over the ~82% level observed in this study, while offering substantial time and cost savings compared to having to prepare and compositionally analyze over 200 samples.

### 5.2. Pegmatite Discrimination

Garnet is widespread in geochemically primitive to rare-element enriched granitic pegmatites of the LCT family, but also occurs in NYF pegmatites [44]. Analyses of garnet from LCT granitic pegmatites typically correspond to almandine and spessartine compositions with minor, but variable Mg and Ca contents [45]. Pegmatite garnets with high percentages of pyrope, grossular or andradite components are usually the result of local contamination

of the pegmatite melt by carbonate wall rocks [46]. In LCT pegmatites, almandine is regularly observed in poorly evolved pegmatites of simple mineralogy, whereas spessartine is more common in highly fractionated Li-enriched pegmatites. Within individual zoned pegmatites, garnet may occur in multiple generations, with compositions varying from predominantly almandine in the early crystallizing outermost zones and units, to spessartine in interior and later more differentiated units dominated by albite- and Li-mica-bearing assemblages. In REE-enriched NYF granitic pegmatites, Mn-rich almandine is most likely to occur as the dominant garnet species, whereas spessartine predominates in massive, non-miarolitic amazonite-bearing NYF pegmatites and rarely in miarolitic cavities even where Li-mineralization is absent. The second objective of this study was to ascertain if garnets occurring in LCT pegmatites could be distinguished from those present in their NYF counterparts.

Figure 8 shows PCA plots for the RT-100 and Z-500 LIBS analyses for garnets occurring in LCT and NYF granitic pegmatites. The variance in data is similar for both instruments with 51.0%, 15.7% and 8.1% versus 52.4%, 19.0% and 6.7% for the three principal components of the RT-100 and Z-500 data sets, respectively. Neither data set permits clear differentiation of LCT-affiliated garnet from NYF type garnets. However, the Z-500 LIBS data does effectively discriminate between almandine and spessartine garnet across both pegmatite types. Furthermore, the separate PCA plots of garnet from LCT and NYF pegmatites shown in Figure 9 demonstrate that LIBS analysis successfully distinguishes single pegmatite bodies (e.g., Little 3, Ruggles localities) and pegmatite groups (e.g., Amelia, Spruce Pine localities). The PCA plots also reasonably separates metamorphic-affiliated garnet from pegmatite-generated garnets. For both LCT and NYF in the PCA plots, the garnet data highlights the change in garnet composition as it relates to increasing mineral and chemical complexity of the pegmatites via chemical fractionation. In our dataset, almandine is associated with muscovite-rich pegmatites (e.g., Spruce Pine district), pegmatites hosting significant uranium and/or phosphate minerals (e.g., Ruggles locality) to the primitive units/zones of beryl-columbite- and spodumene-bearing pegmatites (Governador Valadares locality). Fe-rich spessartine occurs in the albite-rich, beryl-bearing Weld pegmatite to elbaite- and lepidolite-bearing pegmatites of Minas Gerais, whereas near end-member spessartine resides in the topaz-bearing Little 3 pegmatite and the NYF-affiliated amazonite- and topaz-bearing pegmatites of the Amelia pegmatite district.

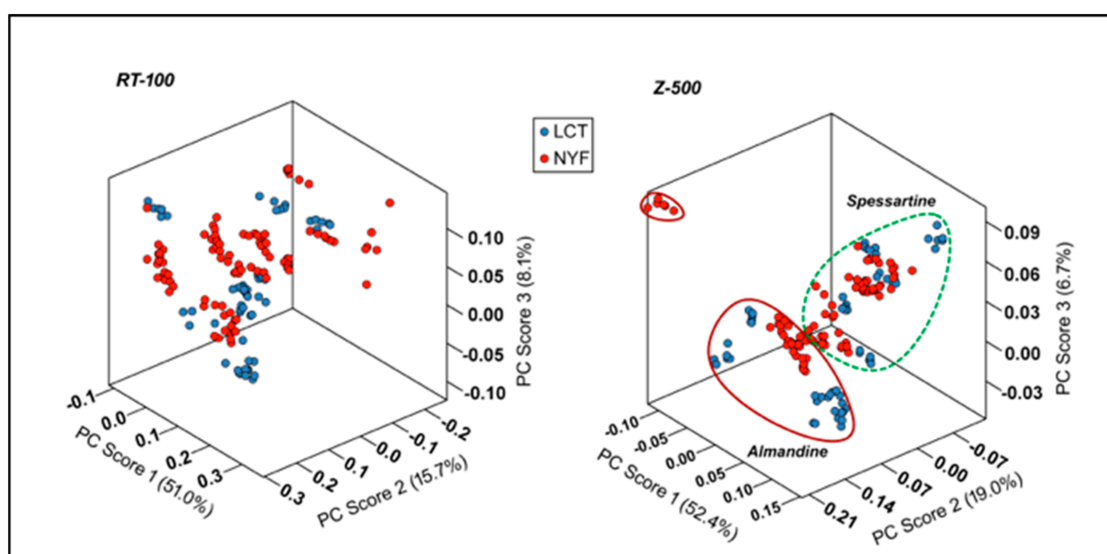


**Figure 8.** PCA scores plots for processed LIBS broadband spectra for garnets from 10 LCT pegmatites and 17 NYF pegmatites (Table A2, Appendix A) acquired with the RT-100 laboratory LIBS system (left) and Z-500 handheld LIBS analyzer (right) showing the compositional distinction of almandine and spessartine garnets. The green dashed lines enclose spessartine garnets, and the solid red lines enclose almandine garnets.

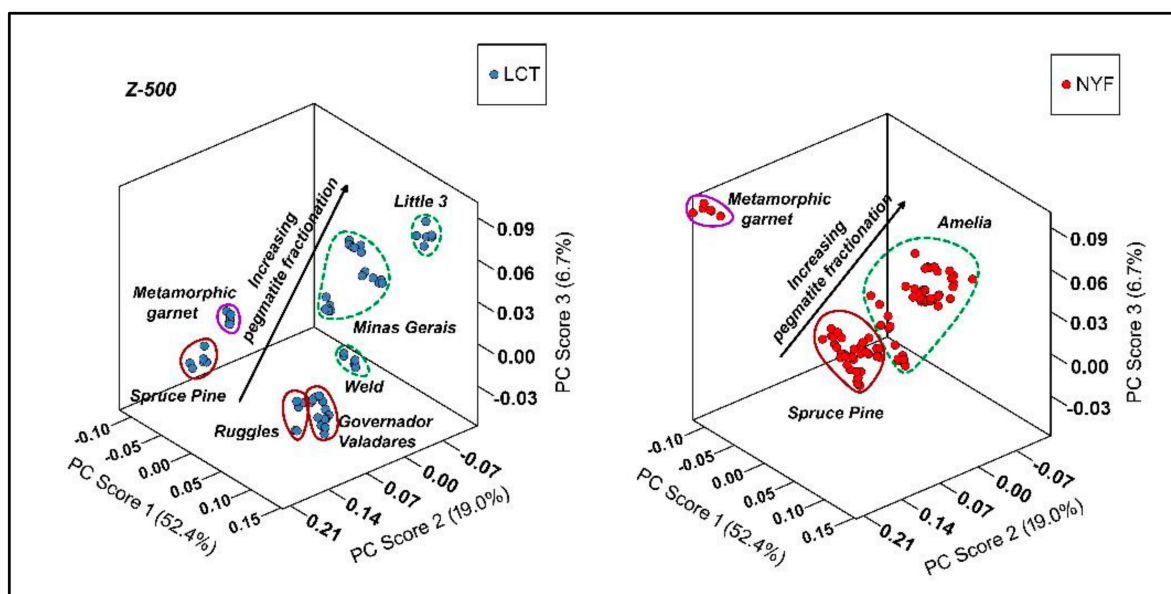


**Figure 9.** PCA scores plots for processed LIBS broadband spectra for garnets from 10 LCT pegmatites and 17 NYF pegmatites (Table A2, Appendix A) acquired with the Z-500 handheld analyzer showing the unique compositional character of garnets from pegmatites of different degrees of chemical fractionation. The green dashed lines enclose spessartine garnets, and the solid red and purple lines enclose almandine garnets.

## 6. Summary and Future Work

The capability to obtain geochemical information outside of the confines of the traditional laboratory setting using handheld analyzers has been one of most important recent technological advancements in analytical chemistry. Laser-induced breakdown spectroscopy (LIBS) is an established technique of analytical atomic spectrometry that today offers, in handheld analyzer form, a convenient, reliable, and versatile technique for localized material analysis. The application of both laboratory and handheld LIBS across multiple domains of the geosciences has been described in the literature (see e.g., [47–56] and references therein). LIBS has a persuasive set of advantages that include its sensitivity to all elements, particularly the light elements ( $Z < 20$ ) that cannot be analyzed by other field-portable methods; its capability to analyze material in any state—solid, liquid, or gas with little to no sample preparation; and its ability for rapid analysis in situ under ambient environmental conditions. Additionally, LIBS affords high spatial resolution analysis for lateral and depth compositional profiling. Here we have considered the use of LIBS spectral analysis, used in conjunction with chemometric techniques and pre-established databases, to identify and discriminate unknown materials in two possible contexts outside the laboratory—in a museum mineral collection to rapidly identify mislabeled specimens in real time and geological exploration fieldwork to recognize and distinguish garnets from LCT and NYF pegmatites.

Utilizing a collection that consisted of 42 almandines, 40 andradites, 54 grossulars, 18 pyropes, 48 spessartines, and 6 uvarovites that originated from a wide range of igneous and metamorphic rock associations and were analyzed by both a laboratory LIBS system and a handheld LIBS analyzer, we were able to ascertain based on actual chemical compositions determined by EMP analysis, that over 17% of the 208 samples had been incorrectly labeled. Through PCA, we observed that the six garnet types are differentiated by three vectors denoting the solid solution of divalent cations in the dodecahedral X structural site and octahedral trivalent cations in Y structural site that have different geometric orientations in the PCA plots and concluded that LIBS analysis is effective in discriminating the six common garnet species based on their major element composition. Overall chemometric analysis by SVM was equivalent to PLSDA for garnet discrimination for both the laboratory LIBS and handheld LIBS data sets. Through the application of PCA to the subset of spectral

data for 27 pegmatite garnets (10 having LCT associations and 17 having NYF associations), we were able to distinguish spessartine and from almandine and discriminate pegmatite localities characterized by different degrees of parent melt chemical fractionation.

A demonstration effort is planned to validate the museum labeling study presented here for garnet type discrimination. This follow-on study will use a handheld LIBS analyzer to examine an entire museum collection of garnets, using either the >800 specimens in the mineralogy collection of the Yale Peabody Museum of Natural History or the >3500 specimens in the mineralogy collection of the Nation Museum of Natural History. Each sample in the collection would be analyzed and assigned a type-label based upon a comparison against the spectral library developed from this study of 208 garnets of known composition. These labels would be validated by subsequently analyzing a random selection of samples by quantitative chemical analysis by either electron microprobe or X-ray fluorescence analysis. Additional work also should be carried out to ensure that the LIBS spectra collected are representative of the bulk composition using tools such as spectral similarity index or intensity filters [57]. It will also be helpful to acquire spectra from a larger number of locations. This approach will help ensure that in those cases where substantial heterogeneity exists electron microprobe can be used to classify the sample with greater confidence.

Granitic pegmatites can host a variety of minerals that look similar in outcrop or hand samples and are difficult to distinguish visually. Handheld LIBS units could be a powerful tool for rapidly distinguishing different black (e.g., biotite, columbite group minerals, wodginite, cassiterite, hornblende or augite), white (e.g., albite, petalite, pollucite, quartz), green (e.g., apatite, elbaite, gahnite), or pink minerals (e.g., elbaite, almandine-spessartine) in the field. The rapid identification of common and accessory pegmatite minerals using a field-portable LIBS instrument may prove to be a powerful tool in exploration programs attempting to identify pegmatites that may be potential sources of critical minerals.

**Author Contributions:** The research framework for this study was designed by M.A.W., R.S.H. and R.R.H., with the chemometric analysis portion of the effort designed and executed by P.A.D.; the analytical work discussed here was divided into three parts: M.A.W. undertook the EMP analyses, the LIBS RT-100 analytical work was conducted by P.A.D. and the Z-500 analyses were carried out by K.H., both under the supervision of R.R.H.; M.A.W. was responsible for Section 2, M.A.W. and R.S.H. for Section 3, M.A.W., R.R.H. and R.S.H. for Section 4, and M.A.W., R.S.H., R.R.H. and P.A.D. for Section 5; the original draft was written by R.S.H. and M.A.W., supported by P.A.D. and R.R.H. All authors have read and agreed to the published version of the manuscript.

**Funding:** This research received no external funding.

**Data Availability Statement:** The LIBS spectra for all of the samples described in this paper are archived in the LIBS Garnet Analysis folder on the Open Science Framework tool (<https://osf.io/UJA9W/>), accessed on 15 May 2021).

**Acknowledgments:** We thank the Smithsonian National Museum of Natural History for the access provided to its garnet mineral collection and express our appreciation to D. Sackett and D. Day of SciAps, Inc. for providing the Z-500 handheld LIBS analyzer used in this study.

**Conflicts of Interest:** The authors declare no conflict of interest.

## Appendix A

Table A1. Garnet Sample Suite.

Catalog Number	Original Sample Label	EM-Based Identification	Locality
<b>Almandine</b>			
RH-16	Alm	Alm	Roxbury, Litchfield Co., Connecticut, USA
RH-17	Alm	Alm	Roxbury, Litchfield Co., Connecticut, USA
RH-18	Alm	Alm	Roxbury, Litchfield Co., Connecticut, USA
RH-19	Alm	Alm	Roxbury, Litchfield Co., Connecticut, USA
RH-22	Alm	Alm	South Glastonbury, Hartford Co., Connecticut, USA
RH-39	Sps	Alm	Garnet Hill, White Pine Co., Nevada, USA
RH-41	Alm	Alm	Serrote Redondo, Paraiba State, Brazil
RH-44	Alm	Alm	Altay, Xinjiang, China
RH-45	Sps	Alm	Ely (nearby), White Pine Co., Nevada, USA
RH 53	(?)	Alm	Erongo Mountains, Erongo Region, Namibia
RH-60	Alm	Alm	Sedalia Mine near Salida, Chaffee Co., Colorado, USA
RH-66	(?)	Alm	Nagar Valley, Northern Pakistan, Pakistan
RH-68	Alm	Alm	Kievu, Kola Peninsula, Russia
RH-70	Grs	Alm	Gejiu, Yunnan, China
RH-80	Alm	Alm	Bella Vista Claim, Alaska Garnet Mines, Petersburg Borough, Alaska, USA
NMNH-17909	Alm	Alm	Thorn Mountain, Macon Co., North Carolina, USA
NMNH-74986	Alm	Alm	Roxbury, Litchfield Co., Connecticut, USA
NMNH-80219	Alm	Alm	Ray Mica Mine, Yancey Co., North Carolina, USA
NMNH-82575	Prp	Alm	Bilina, Ústí nad Labem Region, Czech Republic
NMNH-90518	Alm	Alm	H.H. Barton & Sons Company mine, Gore Mountain, Warren Co., New York, USA
NMNH-104496	Alm	Alm	Ötztal, Tyrol, Austria
NMNH-106097	Sps	Alm	Golconda Mine, Minas Gerais State, Brazil
NMNH-107060	Alm	Alm	Schneeberg, Tyrol, Austria
NMNH-107061	Alm	Alm	Zillertal, Tyrol, Austria
NMNH-107089	Alm	Alm	Roxbury, Litchfield Co., Connecticut, USA
NMNH-107140	Alm	Alm	Mink's Pond, Grafton Co., New Hampshire, USA
NMNH-107142	Alm	Alm	Brooklyn Tunnel, Manhattan, New York, USA
NMNH-114216	Alm	Alm	Penland, Mitchell Co., North Carolina, USA
NMNH-132542	Alm	Alm	Roxbury, Litchfield Co., Connecticut, USA
NMNH-132686	Alm	Alm	Gassetts, Windsor Co., Vermont, USA
NMNH-134685	Alm	Alm	Ruggles Mine, Grafton, Grafton Co., New Hampshire, USA
NMNH-143894	Prp	Alm	Tanzania
NMNH-166062	Alm	Alm	Chestnut Flats mine, Burnsville, Mitchell Co., North Carolina, USA
NMNH-166064	Alm	Alm	Chestnut Flats mine, Burnsville, Mitchell Co., North Carolina, USA
NMNH-B19430	Alm	Alm	Ötztal, Tyrol, Austria
NMNH-C2779	Alm	Alm	Zillertal, Tyrol, Austria
NMNH-C2780	Alm	Alm	Schwarzenstein, Tyrol, Austria
NMNH-C5331-1	Sps	Alm	Topaz Mountain, Juab Co., Utah, USA
NMNH-C5331-2	Sps	Alm	Topaz Mountain, Juab Co., Utah, USA
NMNH-R16774	Sps	Alm	Governador Valadares, Minas Gerais State, Brazil
NMNH-R3429	Alm	Alm	Roxbury, Litchfield Co., Connecticut, USA (chlorite schist)
NMNH-R3429	Alm	Alm	Roxbury, Litchfield Co., Connecticut, USA (muscovite schist)

Table A1. Cont.

Catalog Number	Original Sample Label	EM-Based Identification	Locality
<b>Pyrope</b>			
RH-75	Adr	Prp	Mutumba, Madagascar
RH-76	Prp	Prp	Umba River Valley, Tanzania/Kenya
RH-77	Prp	Prp	Ivory Coast
RH-81	Prp	Prp	Africa
NMNH-83108	Prp	Prp	Navajo Indian Reservation, Apache Co., Arizona, USA
NMNH-92684	Prp	Prp	Mason Mountain mine, Mason Co., North Carolina, USA
NMNH-107198	Prp	Prp	Navajo Indian Reservation, Apache Co., Arizona, USA
NMNH-107199	Prp	Prp	Třebonice, Bohemia Region, Czech Republic
NMNH-115588	Prp	Prp	Mason Mountain mine, Mason Co., North Carolina, USA
NMNH-120315	Prp	Prp	Navajo Indian Reservation, Apache Co., Arizona, USA
NMNH-122845	Prp	Prp	Garnet Ridge, Apache Co., Arizona, USA
NMNH-128282	Prp	Prp	Monastery Mine, Free State Province, South Africa
NMNH-128285	Prp	Prp	Newlands mine, Barkly West, Northern Cape Province, South Africa
NMNH-128290	Prp	Prp	Kamferdam Mine, Kimberley, Northern Cape Province, South Africa
NMNH-133612	Prp	Prp	Rauhammaren, Åheim, Norway
NMNH-162498	Prp	Prp	Dora Maira Massif, Western Alps, Italy
NMNH-R3418	Prp	Prp	Trziblit, Bohemia Region, Czech Republic
NMNH-R3421	Prp	Prp	Kimberley, Northern Cape Province, South Africa
<b>Spessartine</b>			
RH-24	Adr	Sps	Henson's Branch, Watauga Co., North Carolina, USA
RH-25	Grs	Sps	Ducktown Mine, Polk Co., Tennessee, USA
RH-30	Sps	Sps	Fujian Province, China
RH-40	Sps	Sps	Little 3 Mine, Ramona, San Diego Co., California, USA
RH-55	Sps	Sps	Tongbei, Fujian Province, China
RH-59	Sps	Sps	Tongbei, Fujian Province, China
RH-63	Sps	Sps	Minas Gerais State, Brazil
RH-83	Prp	Sps	Umba River Valley, Tanzania/Kenya
NMNH-48559	Sps	Sps	Nathrop, Chaffee Co., Colorado, USA
NMNH-48559-1	Sps	Sps	Nathrop, Chaffee Co., Colorado, USA
NMNH-48745	Sps	Sps	Amelia, Amelia Co., Virginia, USA
NMNH-48745-1	Sps	Sps	Amelia Court House, Amelia Co., Virginia, USA
NMNH-80457	Sps	Sps	Nathrop, Chaffee Co., Colorado, USA
NMNH-105183	Sps	Sps	Rutherford mine, Amelia, Amelia Co., Virginia, USA
NMNH-107136	Alm	Sps	Gilsum, Cheshire Co., New Hampshire, USA
NMNH-107153	Alm	Sps	Spruce Pine, Mitchell Co., North Carolina, USA
NMNH-107284-1	Sps	Sps	Broken Hill, New South Wales, Australia
NMNH-107286	Sps	Sps	Governador Valadares, Minas Gerais State, Brazil
NMNH-107304	Sps	Sps	Avondale, Delaware Co., Pennsylvania, USA
NMNH-107304-1	Sps	Sps	Avondale, Delaware Co., Pennsylvania, USA
NMNH-114143	Sps	Sps	Rutherford mine, Amelia, Amelia Co., Virginia, USA
NMNH-116955	Sps	Sps	Broken Hill, New South Wales, Australia
NMNH-118214	Alm	Sps	Pine Mountain mine, Spruce Pine, Mitchell Co., North Carolina, USA
NMNH-118215	Alm	Sps	Pine Mountain mine, Spruce Pine, Mitchell Co., North Carolina, USA
NMNH-134521	Sps	Sps	Ermo Mine, Carnaúba Dos Dantas, Rio Grande do Norte, Brazil
NMNH-135296	Sps	Sps	Amelia Court House, Amelia, Rutherford Mine, Virginia, USA
NMNH-135296	Sps	Sps	Rutherford mine, Amelia, Amelia Co., Virginia, USA
NMNH-140187	Sps	Sps	Broken Hill, New South Wales, Australia
NMNH-140200	Sps	Sps	Brazil

Table A1. Cont.

Catalog Number	Original Sample Label	EM-Based Identification	Locality
NMNH-158849	Sps	Sps	Broken Hill, New South Wales, Australia
NMNH-158900	Sps	Sps	Broken Hill, New South Wales, Australia
NMNH-164543	Sps	Sps	Minas Gerais State, Brazil
NMNH-166063	Alm	Sps	Chestnut Flats mine, Spruce Pine, Mitchell Co., North Carolina, USA
NMNH-166829	Sps	Sps	Ash Creek, Pinal Co., Arizona, USA
NMNH-170978	Sps	Sps	Kaokoveld, Kunene Region, Namibia
NMNH-174389	Sps	Sps	Amelia, Amelia Co., Virginia, USA
NMNH-B19543	Sps	Sps	Nathrop, Chaffee Co., Colorado, USA
NMNH-B19547	Sps	Sps	Nathrop, Chaffee Co., Colorado, USA
NMNH-C2719	Sps	Sps	Broken Hill, New South Wales, Australia
NMNH-C2726	Sps	Sps	Nathrop, Chaffee Co., Colorado, USA
NMNH-R3437	Sps	Sps	Broken Hill, New South Wales, Australia
NMNH-R3448	Sps	Sps	Allen Mica mine, Amelia, Amelia Co., Virginia, USA
NMNH-R3469	Adr	Sps	Franklin Mine, Sussex Co., New Jersey, USA
NMNH-R6771	Sps	Sps	Amelia, Amelia Co., Virginia, USA
NMNH-R9587	Sps	Sps	Nathrop, Chaffee Co., Colorado, USA
NMNH-R11280	Sps	Sps	Broken Hill, New South Wales, Australia
NMNH-R14530	Sps	Sps	Nathrop, Chaffee Co., Colorado, USA
WELD-2	Sps	Sps	Weld, Franklin Co., Maine, USA
<b>Grossular</b>			
RH-15	Grs	Grs	Aosta Valley, Valle d'Aost Autonomous Region, Italy
RH-20	Grs	Grs	Bishop, Inyo Co., California, USA
RH-26	Uv	Grs	Black Lake, Québec, Canada
RH-27	Grs	Grs	Sierra de Cruces, Sierra Mojada municipality, Coahuila, Mexico
RH-29	Grs	Grs	Angola#1, Sibindi Cercle, Kayes Region, Mali
RH-33	Grs	Grs	Coyote Front Range, Bishop, Inyo Co., California, USA
RH-34	Grs	Grs	Cerro El Toro, Sonora State, Mexico
RH-37	Grs	Grs	Jeffrey Mine, Québec, Canada
RH-46	Grs	Grs	Viluy River, Siberia, Russia
RH-49	Grs	Grs	Sierra de Cruces, Sierra Mojada municipality, Coahuila, Mexico
RH-50	Grs	Grs	Havilah, Kern Co., California, USA
RH-51	Grs	Grs	Sierra de Cruces, Sierra Mojada municipality, Coahuila, Mexico
RH-52	Grs	Grs	Sierra de Cruces, Sierra Mojada municipality, Coahuila, Mexico
RH-58	Grs	Grs	Sierra de Cruces, Sierra Mojada municipality, Coahuila, Mexico
RH-61	Grs	Grs	Akhtaragda River, Siberia, Russia
RH-69	Adr	Grs	Mali
NMNH-16321	Adr	Grs	Ural Mountains, Chelyabinsk Oblast, Russia
NMNH-47358	Adr	Grs	Burnet, Burnet Co., Texas, USA
NMNH-103111	Grs	Grs	Yakutia-Sakha Republic, Russia
NMNH-107055	Grs	Grs	Eden Mills, Lamoille Co., Vermont, USA
NMNH-107232-1	Adr	Grs	Nightingale Mining District, Pershing CO., Nevada, USA
NMNH-107260	Adr	Grs	Snohomish, Snohomish Co., Washington, USA
NMNH-112962	Grs	Grs	Eden Mills, Lamoille Co., Vermont, USA
NMNH-117637	Grs	Grs	Eden Mills, Lamoille Co., Vermont, USA
NMNH-121912	Grs	Grs	Sierra de Cruces, Sierra Mojada municipality, Coahuila, Mexico
NMNH-126947	Grs	Grs	Jeffrey Mine, Quebec, Canada
NMNH-127138	Grs	Grs	Eden Mills, Lamoille Co., Vermont, USA
NMNH-132506	Grs	Grs	Eden Mills, Lamoille Co., Vermont, USA

Table A1. Cont.

Catalog Number	Original Sample Label	EM-Based Identification	Locality
NMNH-132617	Grs	Grs	Ruberoid Asbestos mine, Eden Mills, Lamoille Co., Vermont, USA
NMNH-139717	Grs	Grs	Orford, Québec, Canada
NMNH-143887	Grs	Grs	Kimolo Region, Tanzania
NMNH-143961	Hgr	Grs	Buffelsfontein, North West Province, South Africa
NMNH-144275	Grs	Grs	Mwadui Workings, Tanzania
NMNH-145678	Grs	Grs	Sierra de Cruces, Sierra Mojada municipality, Coahuila, Mexico
NMNH-145817	Grs	Grs	Jeffrey Mine, Québec, Canada
NMNH-150761	Hgr	Grs	Commercial quarry, Crestmore, Riverside Co., California, USA
NMNH-153479	Grs	Grs	Jeffrey Mine, Québec, Canada
NMNH-154129	Grs	Grs	Sierra de Cruces, Sierra Mojada municipality, Coahuila, Mexico (green)
NMNH-154129	Grs	Grs	Sierra de Cruces, Sierra Mojada municipality, Coahuila, Mexico (gray)
NMNH-154129	Grs	Grs	Sierra de Cruces, Sierra Mojada municipality, Coahuila, Mexico (pink)
NMNH-154129	Grs	Grs	Sierra de Cruces, Sierra Mojada municipality, Coahuila, Mexico (black)
NMNH-159513	Grs	Grs	Jeffrey Mine, Québec, Canada
NMNH-168752	Cdr	Grs	Katkamsandi, Jharkhand State, India
NMNH-171584	Grs	Grs	Sierra de Cruces, Sierra Mojada municipality, Coahuila, Mexico
NMNH-172138	Grs	Grs	Belvidere mine, Lowell, Orleans Co., Vermont, USA
NMNH-B19516	Adr	Grs	Somma-Vesuvius complex, Naples, Campania, Italy
NMNH-C5946-2	Grs	Grs	Sierra de Cruces, Sierra Mojada municipality, Coahuila, Mexico (pink)
NMNH-C5946-2	Grs	Grs	Sierra de Cruces, Sierra Mojada municipality, Coahuila, Mexico (yellow)
NMNH-R7586-1	Grs	Grs	Sierra Los Muertos, Chihuahua State, Mexico
NMNH-R11362	Grs	Grs	Thetford Mines, Québec, Canada
NMNH-R17257	Grs	Grs	Jeffrey Mine, Quebec, Canada
NMNH-R18145	Grs	Grs	Jeffrey Mine, Québec, Canada
NMNH-R18421	Grs	Grs	Jeffrey Mine, Quebec, Canada
NMNH-R19868	Grs	Grs	Milford, Beaver Co., Utah, USA
<b>Andradite</b>			
RH-31	Adr	Adr	Osgood Mountains, Humboldt Co., Nevada, USA
RH-35	Adr	Adr	N'chwani Mine, Northern Cape Province, South Africa
RH-36	Adr	Adr	Trantimou, Kayes Region, Mali
RH-48	Grs	Adr	Tumiq Tal, Gilgit-Baltistan District, Pakistan
RH-54	Grs	Adr	Erongo Mountains, Erongo Region, Namibia
RH-64	Adr	Adr	Jeffrey Mine, Québec, Canada
RH-65	Adr	Adr	Kirman, Kerman Province, Iran
RH-67	Adr	Adr	Sarbayskii Mine, Kustanay Oblast, Kazakhstan
RH-71	Adr	Adr	Kazakhstan
NMNH-45263	Scm	Adr	Magnet Cove, Hot Spring Co., Arkansas, USA
NMNH-95204	Adr	Adr	Franklin Mine, Sussex Co., New Jersey, USA
NMNH-106348	Adr	Adr	Virginia Lime and Stone Company quarry, Loudon Co., Virginia, USA
NMNH-107251	Adr	Adr	Onca de Fier, Caras-Severin, Romania
NMNH-107258	Adr	Adr	Zermatt, Valais Canton, Switzerland
NMNH-107258-1	Adr	Adr	Zermatt, Valais Canton, Switzerland
NMNH-107314	Uv	Adr	Red Ledge mine, Nevada Co., California, USA
NMNH-112864	Scm	Adr	High Atlas Mountains, Morocco



Table A1. Cont.

Catalog Number	Original Sample Label	EM-Based Identification	Locality
NMNH-113829	Adr	Adr	Zermatt, Valais Canton, Switzerland
NMNH-116725	Adr	Adr	Sondrio, Val Malenco, Lombardy Province, Italy
NMNH-117800	Scm	Adr	Magnet Cove, Hot Spring Co., Arkansas, USA
NMNH-123378	Grs	Adr	Eden Mills, Lamoille Co., Vermont, USA
NMNH-124835	Adr	Adr	Copper Mountain, Prince of Wales Island, Alaska, USA
NMNH-126160	Adr	Adr	Sondrio, Val Malenco, Lombardy Province, Italy
NMNH-143917	Alm	Adr	Schwarzewand, Salzburg, Austria
NMNH-146475	Adr	Adr	Condore, Valle di Susa, Piedmont Province, Italy
NMNH-147797	Grs	Adr	Las Truchas, Oaxaca, Mexico
NMNH-171064	Adr	Adr	La Prieta Linda mine, Chihuahua, Mexico
NMNH-173775	Adr	Adr	Erongo Mountains, Erongo Region, Namibia
NMNH-B19470	Adr	Adr	Zermatt, Valais Canton, Switzerland
NMNH-B19492	Adr	Adr	Onca de Fier, Caras-Severin, Romania
NMNH-B19638	Adr	Adr	Sondrio, Val Malenco, Lombardy Province, Italy
NMNH-C2744	Adr	Adr	Onca de Fier, Caras-Severin, Romania
NMNH-C2763	Adr	Adr	Conway, Carroll County, New Hampshire, USA
NMNH-C6771	Adr	Adr	Franklin Mine, Sussex Co., New Jersey, USA
NMNH-R3467	Adr	Adr	Franklin Mine, Sussex Co., New Jersey, USA
NMNH-R4284	Adr	Adr	Choto Nagpur, Hazaribagh, Bihar, India
NMNH-R17196	Adr	Adr	Chihuahua, Mexico

## Uvarovite

RH-62	Uv	Uv	Saranovskii Mine, Ural Mountains, Russia
NMNH-107315	Uv	Uv	Yermo, San Bernadino Co., California, USA
NMNH-123380	Uv	Uv	Outokumpu, North Karelia, Finland
NMNH-139716	Uv	Uv	Jackson, Amador Co., California, USA
NMNH-161032	Uv	Uv	Outokumpu, North Karelia, Finland
NMNH-C5704	Uv	Uv	Blue Point Claim, Jacksonville, Tuolumne Co., California, USA

Catalog number abbreviations: NMNH—National Museum of Natural History, Smithsonian Institution collection, RH—R. Harmon garnet collection, WELD—Weld pegmatite. Garnet species abbreviations: Alm = almandine, Pyp = pyrope, Sps = spessartine, Grs = grossular, Adr = andradite, Uv = uvarovite, Cdr = calderite, Hgr = hydrogrossular, Scm = schorlomite, (?)—undetermined.

Table A2. Pegmatite Sample List.

Sample ID	EM-Based Classification	Locality
<b>LCT Pegmatites</b>		
RH-40	spessartine	Little 3 Mine, CA, USA
NMNH-80219	almandine	Ray Mica Mine, NC, USA
NMNH-106097	almandine	Golconda Mine, Minas Gerais State, Brazil
NMNH-107140	almandine	Mink's Pond, NH, USA
NMNH-107286	spessartine	Minas Gerais State, Brazil
NMNH-134685	almandine	Ruggle's Mine, NH, USA
NMNH-140200	spessartine	Minas Gerais State, Brazil
NMNH-164543	spessartine	Minas Gerais State, Brazil
NMNH-R16774	almandine	Governador Valadares, Minas Gerais State, Brazil
WELD-2	spessartine	Weld, ME, USA
<b>NYF Pegmatites</b>		
RH-24	spessartine	Henson's Branch, NC, USA
NMNH-48745	spessartine	Amelia Court House, VA, USA
NMNH-48745-1	spessartine	Amelia, VA, USA
NMNH-105183	spessartine	Amelia, VA, USA
NMNH-107153	spessartine	Spruce Pine, NC, USA
NMNH-114143	spessartine	Rutherford Mine, VA, USA
NMNH-114216	almandine	Spruce Pine, NC, USA
NMNH-118214	spessartine	Spruce Pine, NC, USA

Table A2. Cont.

Sample ID	EM-Based Classification	Locality
NMNH-118215	spessartine	Spruce Pine, NC, USA
NMNH-135296	spessartine	Amelia, VA, USA
NMNH-135296	spessartine	Rutherford Mine, VA, USA
NMNH-166062	almandine	Chestnut Flats, NC, USA
NMNH-166063	spessartine	Spruce Pine, NC, USA
NMNH-166064	almandine	Spruce Pine, NC, USA
NMNH-174389	spessartine	Amelia, VA, USA
NMNH-C5278	almandine	Hawk Mine, NC, USA
NMNH-R6771	spessartine	Amelia, VA, USA

## References

1. Cremers, D.A.; Radziemski, L.J. (Eds.) *Handbook of Laser Induced Breakdown Spectroscopy*, 2nd ed.; John Wiley and Sons: Chichester, UK, 2013.
2. Harmon, R.S.; Remus, J.; McMillan, N.J.; McManus, C.; Collins, L.; Gottfried, J.L.; DeLucia, F.C.; Miziolek, A.W. LIBS analysis of geomaterials: Geochemical fingerprinting for the rapid analysis and discrimination of minerals. *Appl. Geochem.* **2009**, *24*, 1125–1141. [[CrossRef](#)]
3. Deer, W.A.; Howie, R.A.; Zussman, J. *An Introduction to the Rock-Forming Minerals*; Longman Scientific: New York, NY, USA, 1992; p. 696, ISBN 139780582300941.
4. Baxter, E.F.; Caddick, M.J.; Ague, J.J. Garnet: Common mineral, uncommonly useful. *Elements* **2013**, *9*, 415–419. [[CrossRef](#)]
5. Morton, A.C. A new approach to provenance studies: Electron microprobe analysis of detrital garnets from Middle Jurassic sandstones of the northern North Sea. *Sedimentology* **1985**, *32*, 553–566. [[CrossRef](#)]
6. Hutchison, A.R.; Oliver, G.J.H. Garnet provenance studies, juxtaposition of Laurentian marginal terranes and timing of the Grampian Orogeny in Scotland. *J. Geol. Soc.* **1998**, *155*, 541–550. [[CrossRef](#)]
7. Krippner, A.; Meinhold, G.; Morton, A.C.; von Eynatten, H. Evaluation of garnet discrimination diagrams using geochemical data of garnets derived from various host rocks. *Sediment. Geol.* **2014**, *306*, 36–52. [[CrossRef](#)]
8. Suggate, S.M.; Hall, R. Using detrital garnet compositions to determine provenance: A new compositional database and procedure. *Geol. Soc. Spec. Publ.* **2014**, *386*, 373–393. [[CrossRef](#)]
9. Griffin, W.L.; Ryan, C.G. Trace elements in indicator minerals: Area selection and target evaluation in diamond exploration. *J. Geochem. Explor.* **1995**, *53*, 311–337. [[CrossRef](#)]
10. Gurney, J.J.; Zweistra, P. The interpretation of the major element compositions of mantle minerals in diamond exploration. *J. Geochem. Explor.* **1995**, *53*, 293–309. [[CrossRef](#)]
11. Grütter, H.S.; Gurney, J.J.; Menzies, A.H.; Winter, F. An updated classification scheme for mantle-derived garnet, for use by diamond explorers. *Lithos* **2004**, *77*, 841–857. [[CrossRef](#)]
12. Hardman, M.F.; Pearson, D.G.; Stachel, T.; Sweeney, R.J. Statistical approaches to the discrimination of mantle- and crust-derived low-Cr garnets using major and trace element data. *Mineral. Petrol.* **2018**, *112*, 697–706. [[CrossRef](#)]
13. Meinert, L.D. Application of skarn deposit zonation models to mineral exploration. *Explor. Min. Geol.* **1997**, *6*, 185–208.
14. Park, C.; Choi, W.; Kim, H.; Park, M.H.; Kang, I.M.; Lee, H.S.; Song, Y. Oscillatory zoning in skarn garnet: Implications for tungsten ore exploration. *Ore Geol. Rev.* **2017**, *89*, 1006–1018. [[CrossRef](#)]
15. Yu, F.; Shu, Q.; Niu, X.; Xing, K.; Li, L.; Lentz, D.R.; Zeng, Q.; Yang, W. Composition of garnet from the Xianghualing Skarn Sn Deposit, South China: Its petrogenetic significance and exploration potential. *Minerals* **2020**, *10*, 456. [[CrossRef](#)]
16. Linnen, R.L.; Van Lichtenvelde, M.; Černý, P. Granitic pegmatites as sources of strategic metals. *Elements* **2012**, *8*, 275–280. [[CrossRef](#)]
17. Černý, P.; Ercit, T.S. The classification of granitic pegmatites revisited. *Can. Mineral.* **2005**, *4*, 2005–2026.
18. Bradley, D.C.; McCauley, A.D.; Stillings, L.L. Mineral-deposit model for lithium-cesium-tantalum pegmatites. In *Mineral Deposit Models for Resource Assessment*; Scientific Investigations Report 2010-5070-O; US Geological Survey: Reston, VA, USA, 2017; p. 40.
19. Ercit, T.S. Identification and alteration trends of granitic-pegmatite-hosted (Y, REE, U, Th)-(Nb, Ta, Ti) oxide minerals: A statistical approach. *Can. Mineral.* **2005**, *43*, 1291–1303. [[CrossRef](#)]
20. Geller, S. Crystal chemistry of the garnets. *Z. Kristallog.* **1967**, *125*, 1–47. [[CrossRef](#)]
21. Menzer, G. The crystal structure of garnet. *Z. Kristallog.* **1928**, *69*, 300–396. [[CrossRef](#)]
22. Grew, E.S.; Locock, A.J.; Mills, S.J.; Galuskina, I.O.; Galuskin, E.V.; Hålenius, U. Nomenclature of the garnet supergroup. *Am. Mineral.* **2013**, *98*, 785–811. [[CrossRef](#)]
23. Rossman, G.R. The geochemistry of gems and its relevance to gemology: Different traces, different prices. *Elements* **2009**, *5*, 159–162. [[CrossRef](#)]
24. Alvey, D.C.; Morton, K.; Harmon, R.S.; Gottfried, J.L.; Remus, J.J.; Collins, L.M.; Wise, M.A. Laser-induced breakdown spectroscopy-based geochemical fingerprinting for the rapid analysis and discrimination of minerals: The example of garnet. *Appl. Opt.* **2010**, *49*, C168–C180. [[CrossRef](#)]

25. Harmon, R.S.; Hark, R.R.; Throckmorton, C.S.; Rankey, E.C.; Wise, M.A.; Somers, A.M.; Collins, L.M. Geochemical fingerprinting by handheld laser-induced breakdown spectroscopy. *Geostand. Geoanal. Res.* **2017**, *41*, 563–584. [CrossRef]
26. Kramida, A.; Ralchenko, Y.; Reader, J.; NIST ASD Team. *NIST Atomic Spectra Database (Version 5.5.6)*; National Institute of Standards and Technology: Gaithersburg, MD, USA, 2018. Available online: <https://physics.nist.gov/asd> (accessed on 3 May 2021).
27. Kenneth, R.B.; Randy, J.P.; Seasholtz, M.B. *Chemometrics: A Practical Guide*; John Wiley and Sons: New York, NY, USA, 1998.
28. Sobron, O.; Wang, A.; Sobron, F. Extraction of compositional and hydration information of sulfates from laser-induced plasma spectra recorded under Mars atmospheric conditions—Implications for ChemCam investigations on Curiosity rover. *Spectrochim. Acta Part B* **2012**, *68*, 1–16. [CrossRef]
29. Duda, R.O.; Hart, P.E.; Stork, D.G. *Pattern Classification*; Wiley Interscience: Chichester, UK, 2001; p. 680, ISBN 9780471056690.
30. Novak, G.A.; Gibbs, G.V. The crystal chemistry of the silicate garnets. *Am. Mineral.* **1971**, *56*, 91–825.
31. Back, M.E.; Mandarino, J.A. *Fleischer's Glossary of Mineral Species 2008*, 10th ed.; Mineralogical Record Inc.: Tucson, AZ, USA, 2008; 346p.
32. Locock, A.J. An Excel spreadsheet to recast analyses of garnet into end-member components, and a synopsis of the crystal chemistry of natural silicate garnets. *Comput. Geosci.* **2008**, *34*, 1769–1780. [CrossRef]
33. Brady, J.; Perkins, D. Mineral Formulae Recalculation. In Teaching Phase Equilibria. 2017. Available online: [https://serc.carleton.edu/research\\_education/equilibria/mineralformulaerecalculation.html](https://serc.carleton.edu/research_education/equilibria/mineralformulaerecalculation.html) (accessed on 13 April 2021).
34. Yavuz, F.; Yildirim, D.K. WinGrt, a Windows program for garnet supergroup minerals. *J. Geosci.* **2020**, *65*, 71–95. [CrossRef]
35. Wold, S.; Esbensen, K.; Geladi, P. Principal component analysis. *Chemometr. Intell. Lab. Syst.* **1987**, *2*, 37–52. [CrossRef]
36. Barker, M.; Rayens, W. Partial least squares for discrimination. *J. Chemom.* **2003**, *17*, 166–173. [CrossRef]
37. Mehmood, T.; Liland, K.H.; Snipen, L.; Sæbø, S. A review of variable selection methods in partial least squares regression. *Chemometr. Intell. Lab. Syst.* **2012**, *118*, 62–69. [CrossRef]
38. Wold, S.; Sjöström, M.; Eriksson, L. PLS-regression: A basic tool of chemometrics. *Chemometr. Intell. Lab. Syst.* **2001**, *58*, 109–130. [CrossRef]
39. Vapnik, V. *The Nature of Statistical Learning Theory*; Springer-Verlag: New York, NY, USA, 1995; p. 314, ISBN 139780387987804.
40. Durgesh, K.S.; Lekha, B. Data classification using support vector machine. *J. Theor. Appl. Inf. Technol.* **2010**, *12*, 1–7.
41. Zhu, X.; Xu, T.; Lin, Q.; Liang, L.; Niu, G.; Lai, H.; Xu, M.; Wang, X.; Li, H.; Duan, Y. Advanced statistical analysis of laser-induced breakdown spectroscopy data to discriminate sedimentary rocks based on Czerny–Turner and Echelle spectrometers *Spectrochim. Acta Part B* **2014**, *93*, 8–13. [CrossRef]
42. Boucher, T.F.; Ozanne, M.V.; Carmosino, M.L.; Dyar, M.D.; Mahadevan, S.; Breves, E.A.; Lepore, K.H.; Clegg, S.M. A study of machine learning regression methods for major elemental analysis of rocks using laser-induced breakdown spectroscopy. *Spectrochim. Acta Part B* **2015**, *107*, 1–10. [CrossRef]
43. Shi, Q.; Niu, G.; Lin, Q.; Xu, T.; Li, F.; Duan, Y. Quantitative analysis of sedimentary rocks using laser-induced breakdown spectroscopy: Comparison of support vector regression and partial least squares regression chemometric methods. *J. Anal. At. Spectrom.* **2015**, *30*, 2384–2393. [CrossRef]
44. Černý, P.; London, D.; Novák, M. Granitic pegmatites as reflections of their sources. *Elements* **2012**, *8*, 289–294. [CrossRef]
45. Černý, P.; Hawthorne, F.C. Selected peraluminous minerals. *Mineral. Assoc. Can. Short Course Handb.* **1982**, *8*, 163–186.
46. Kasowski, M.A.; Hogarth, D.D. Yttrian andradite from the Gatineau Park, Quebec. *Can. Mineral.* **1968**, *9*, 552–558.
47. Lee, Y.I.; KSong, K.; Sneddon, J. *Laser-Induced Breakdown Spectrometry*; Nova Publishers, Hauppauge: New York, NY, USA, 2000; p. 194.
48. Miziolek, A.W.; Palleschi, V.; Schechter, I. (Eds.) *Laser Induced Breakdown Spectroscopy*; Cambridge University Press: Cambridge, UK, 2006; p. 314.
49. Singh, J.P.; Thakur, S.N. (Eds.) *Laser-Induced Breakdown Spectroscopy*; Elsevier: Amsterdam, The Netherlands, 2007; p. 624.
50. Hahn, D.W.; Omenetto, N. Laser-induced breakdown spectroscopy (LIBS), Part I: Review of basic diagnostics and plasma–particle interactions: Still-challenging issues within the analytical plasma community. *Appl. Spectrosc.* **2010**, *64*, 335A–366A. [CrossRef] [PubMed]
51. Hahn, D.W.; Omenetto, N. Laser-induced breakdown spectroscopy (LIBS), Part II: Review of instrumental and methodological approaches to material analysis and applications to different fields. *Appl. Spectrosc.* **2012**, *66*, 347–419. [CrossRef]
52. Cremers, D.A.; Radziemski, L.J. *Handbook of Laser-Induced Breakdown Spectroscopy*; Wiley: Hoboken, NJ, USA, 2013; p. 314.
53. Musazzi, S.; Perini, U. (Eds.) *Laser-Induced Breakdown Spectroscopy, Theory and Applications*; Springer: New York, NY, USA, 2014; p. 577.
54. Fabre, C. Advances in Laser-Induced Breakdown Spectroscopy analysis for geology: A critical review. *Spectrochim. Acta B* **2020**, *166*, 105799. [CrossRef]
55. Senesi, G.S.; Harmon, R.S.; Hark, R.R. Field-portable and handheld LIBS: Historical review, current status and future prospects. *Spectrochim. Acta B* **2020**, *175*, 106013. [CrossRef]
56. Harmon, R.S.; Senesi, G.S. Laser-Induced Breakdown Spectroscopy—A geochemical tool for the 21st century. *Appl. Geochem.* **2021**, *128*, 104929. [CrossRef]
57. Harmon, R.S.; Throckmorton Hark, R.R.; Gottfried, J.L.; Wörner, G.; Harpp, K.; Collins, L. Discriminating volcanic centers with handheld laser-induced breakdown spectroscopy (LIBS). *J. Archaeol. Sci.* **2018**, *98*, 112–127. [CrossRef]